Aus der Klinik für Zahnärztliche Prothetik und Werkstoffkunde

Universitätsklinikum des Saarlandes, Homburg/ Saar

Klinikdirektor: Prof. Dr. Matthias Karl

Bone damage during dental implant insertion –

a pilot study combining strain gauge

and histologic analysis

Knochenschädigung im Rahmen der Implantatinsertion –

eine biomechanische und histologische Pilotstudie

vorgelegt von:

Virgilia Caroline Klär

geb. am 16.11.1998 in Saarbrücken

Tag der Promotion: 18.07.2023

Dekan: Prof. Dr. M. D. Menger

1. Berichterstatter: Prof. Dr. M. Karl

2. Berichterstatter: Prof. Dr. M. W. Laschke

In Liebe für meine Familie

Table of contents

List of figures

List of tables

List of abbreviations

Abbreviation	Meaning	Unit
BICc	Bone to implant contact in the cortical area	[%]
BICt	Bone to implant contact in the trabecular area	[%]
BMDc	Bone mineral density in the cortical area	[%]
BMDt	Bone mineral density in the trabecular area	[%]
defC	Number of deformed bone areas detected in cortical bone	[quantity]
defT	Number of deformed bone areas detected in trabecular bone	[quantity]
ISQ	Implant stability quotient	[no physical unit]
IT, Torque	Implant insertion torque	[Ncm]
macroC	Number of macrocracks detected in cortical bone	[quantity]
macroT	Number of macrocracks detected in trabecular bone	[quantity]
microC	Number of microcracks detected in cortical bone	[quantity]
microT	Number of microcracks detected in trabecular bone	[quantity]
RFA	Resonance frequency analysis	-
ROI	Region of interest	-
SD	Standard deviation	-
Strain	Strain development on buccal bone	[μm/m]
vs.	versus	-

1 Abstract

1.1 English summary

Aim: Achieving primary implant stability during implant placement is an important factor in attaining osseointegration, which determines the long-term clinical success of dental implants. Primary stability is largely dependent on the quality of the alveolar bone as well as the implant design with its specific drilling protocol. Due to the creation of a drill hole as well as cortical bone compression during implant placement, traumatization of the bone appears unavoidable. To reduce the extent of marginal bone resorption, implant manufacturers as well as implantologists try to minimize the traumatic bone damage during the implantation procedure. The aim of this in vitro study was to measure the forces acting on the alveolar bone during the insertion of two different implant systems, to evaluate the extent of bone damage by means of a subsequent histological analysis and to establish possible correlations.

Material and Methods: Implants of two bone-level systems (Astra; Straumann; n = 5) were inserted into fresh bovine bone. The insertion torque was recorded with the surgical contra-angle handpiece. Strain gauges were used to monitor the resulting bone strain on the buccal wall. Subsequently, primary stability of the implant was determined by means of Osstell measurement. Histological analysis determined bone to implant contact and bone density as well as signs of bone damage such as microcracks, macrocracks and the extent of bone deformation. In addition to comparing the implant systems (Welch *t*-Tests), all measurement parameters were tested for possible correlations (Pearson product moment correlation coefficient), with the level of significance set at $\alpha = 0.05$.

Results: Straumann implants produced slightly increased readings for insertion torque (p = 0.772), strain development (p = 0.893) and primary implant stability (p = 0.642). Histologic assessment revealed significantly increased bone to implant contact in the Straumann group compared to the Astra group (cortical p = 0.014; trabecular p = 0.016), with only slight differences in bone density (cortical p = 0.466; trabecular p = 0.360). A significantly increased number of microcracks in the cortical bone was observed in the Astra group (p = 0.020). A correlation of insertion torque with bone to implant contact in cortical bone (p = 0.029) was found in the Straumann group. In trabecular bone, the number of macrocracks correlated with bone to implant contact (p = 0.029). Astra implants showed a correlation of insertion torque with bone to implant contact in the trabecular region (p = 0.007). There was also a correlation between implant stability and the number of macrocracks in the trabecular bone (p = 0.016), furthermore between the number of macrocracks in the cortical region and the bone to implant contact (p = 0.019).

Conclusion: The present study demonstrated that bone damage of varying degrees is inevitable during implant placement. Clinically, they mainly manifest in the peri-implant cortical bone. When developing a new implant macrodesign, attempts should be made to achieve implant stability by compression in the trabecular bone so as to relieve the peri-implant cortical area.

1.2 Zusammenfassung

Ziel: Das Erreichen von Primärstabilität bei der Implantation ist ein wichtiger Faktor zur Erzielung von Osseointegration, was den langfristigen klinischen Erfolg dentaler Implantate bedingt. Die Primärstabilität hängt maßgeblich von der Qualität des Alveolarknochens sowie der Implantatform mit seinem spezifischen Bohrprotokoll ab. Durch das Anlegen eines Bohrstollens sowie durch die kortikale Knochenkompression bei der Implantatinsertion erscheint eine Traumatisierung des Knochens unvermeidbar. Um das Ausmaß einer marginalen Knochenresorption zu verringern, versuchen Implantathersteller sowie Implantologen die traumatische Knochenschädigung während des Implantationsvorganges zu minimieren. Ziel dieser in vitro Studie war es, die während der Insertion zweier verschiedener Implantatsysteme am Alveolarknochen einwirkenden Kräfte messtechnisch zu erfassen, anhand einer anschließenden histologischen Analyse das Ausmaß der Knochenschädigung zu evaluieren und mögliche Zusammenhänge zu erkennen.

Material und Methoden: Die Implantate zweier Bone-Level Systeme (Astra; Straumann; n = 5) wurden in frische Rinderknochen inseriert. Das Eindrehmoment wurde mit dem chirurgischen Winkelstück festgehalten. Mit Hilfe von Dehnungsmessstreifen zeichnete man die dabei an der bukkalen Wand entstehende Knochendehnung auf. Anschließend erfolgte die Bestimmung der Primärstabilität des Implantates mittels Osstell-Messung. In der histologischen Analyse ermittelte man den Knochen-Implantat-Kontakt und die Knochendichte sowie Anzeichen von Knochenschäden wie Mikrorisse, Makrorisse und das Ausmaß der Knochendeformation. Neben dem Vergleich der Implantatsysteme (Welch *t*-Test) wurden alle Messparameter auf mögliche Korrelationen untersucht (Pearson Produkt-Moment-Korrelationskoeffizient), wobei das Signifikanzniveau auf $\alpha = 0.05$ festgelegt wurde.

Ergebnisse: Straumann-Implantate wiesen leicht erhöhte Messwerte für das Eindrehmoment (p = 0.772), die Knochendehnung (p = 0.893) und die Primärstabilität (p = 0.642) auf. Die histologische Beurteilung erbrachte einen signifikant größeren Knochen-Implantat-Kontakt der Straumann Gruppe im Vergleich zur Astra Gruppe (kortikal p = 0.014; trabekulär p = 0.016), wobei sich die Knochendichte nur gering unterschied (kortikal p = 0.466; trabekulär p = 0.360). Eine signifikant erhöhte Zahl an Mikrorissen im kortikalen Knochen fand sich bei den Astra-Implantaten (p = 0.020). Eine Korrelation des Eindrehmomentes mit dem Knochen-Implantat-Kontakt im kortikalen Knochen (p = 0.029) ergab sich in der Straumann Gruppe. Im trabekulären Knochen korrelierte die Anzahl der Makrorisse mit dem Knochen-Implantat-Kontakt (p = 0.029). Bei Astra-Implantaten fand sich eine Korrelation des Eindrehmomentes mit dem Knochen-Implantat-Kontakt im trabekulären Bereich (p = 0.007). Auch zwischen der Implantatstabilität und der Anzahl der Makrorisse im trabekulären Knochen bestand eine Korrelation (p = 0.016), weiterhin zwischen der Anzahl der Makrorisse im kortikalen Bereich und dem Knochen-Implantat-Kontakt (p = 0.019).

Schlussfolgerung: In der vorliegenden Untersuchung konnte gezeigt werden, dass bei der Implantatinsertion Knochenschäden unterschiedlichen Ausmaßes unvermeidlich sind. Klinisch treten sie vornehmlich im peri-implantären kortikalen Knochen in Erscheinung. Bei der Entwicklung eines neuen Implantat-Makrodesigns sollte man daher versuchen, Implantatstabilität durch Kompression im trabekulären Knochen zu erzielen, um den kortikalen Bereich zu entlasten.

2 Introduction

2.1 Fundamentals of implant dentistry

Dental implants constitute an integral part of current treatment concepts and are considered a reliable treatment modality due to their high success rates (Karl & Albrektsson 2017). Modern implant dentistry was mainly established by Per-Ingvar Brånemark who inaugurated screw-type implants and histologically described osseointegration (Brånemark 1983). As part of this work, a list of prerequisites for achieving osseointegration was described. Among others, Brånemark (1983) postulated an adequate preparation of osteotomies minimizing trauma to the jaw bone.

The clinical success of durable implants is based on the knowledge of many different fundamental scientific aspects such as medicine, biomechanics and material science (Misch et al. 2008; Trisi et al. 2013). It is certain that intraosseous implant mobility, due to connective tissue, bone remodeling or bone resorption may lead to implant failure (Misch et al. 2008). Hence, implants must be firmly anchored in bone in order to achieve adequate osseointegration and functionality (Cha et al. 2015). This phenomenon of implant stability is basically differentiated in primary implant stability and secondary implant stability. Primary implant stability is a purely mechanical phenomenon and refers to the mechanical anchoring of the implant directly after insertion (Trisi et al. 2013). It depends on different factors such as bone structure (Lekholm & Zarb 1985), implant design with its micro- and macrogeometry (Karl & Irastorza-Landa 2017) and the surgical procedure, specifically undersizing of the osteotomy (Javed et al. 2013; Dorogoy et al. 2017; Karl & Grobecker-Karl 2018). Secondary implant stability is the outcome of successful osseointegration (Dorogoy et al. 2017). The term osseointegration refers to direct contact between the implant and healthy bone without fibrous parts or gaps due to bone remodeling (Albrektsson & Johansson 2001). Whereas traditional treatment protocols assumed that only undisturbed healing would lead to secondary implant stability, modern treatment protocols now pursue early/ immediate loading to implants in order to shorten treatment times (Donati et al. 2008; Susarla et al. 2008; Donos et al. 2021). Nevertheless, as primary implant stability diminishes during healing while secondary implant stability increases, advanced treatment protocols require high levels of primary stability (Coelho et al. 2013; Ikar et al. 2020).

2.2 Primary implant stability

Chen et al. (2019) indicated that there is a higher risk of implant loss when adequate initial implant stability has not been achieved. Primary implant stability may be compared to fracture fixation in order to avoid fibrous encapsulation. It can be evaluated, for example, by insertion torque (IT), resonance frequency analysis (RFA; Osstell ISQ device, Osstell AB, Gothenburg, Sweden) and Periotest® (Medizintechnik Gulden e.K., Modautal, Germany) (Aparicio 1997; Al-Jetaily & Al-Dosari 2011; Lages et al. 2018). Insertion torque means the axial force applied to an apically rotating implant during insertion to overcome bone resistance (Baldi et al. 2018) and depends, for example, on the bone density

and quality (Bayarchimeg et al. 2013; Trisi et al. 2013; Karl et al. 2020) as well as implant design and surface characteristics (Dos Santos et al. 2011). The implant stability quotient is the result of resonance frequency analysis in which the measured values can vary between 0 as minimum stability and 100 as maximum stability (Baldi et al. 2018). It rates the mobility of the implant, but does not characterize the amount of bone at the contact surface between implant and bone (Gehrke et al. 2019). The Periotest® measures the response of the tissue surrounding the implant to a defined impact load with values ranging from -8 as low mobility to +50 as high mobility (Swami et al. 2016). It is obvious that due to different measurement principles the recording of the techniques mentioned cannot be compared. Insertion torque, for example, depends on quantity and quality of the bone (Bayarchimeg et al. 2013) and is a measurement parameter during surgery and thus only once recordable. The other non-invasive postoperative measurements, however, can be repeated as often as desired. Osstell as well as the Periotest® system proved to be reliable methods, however with the difference that the reliability of the Osstell system may increase with increasing implant stability and that of the Periotest® system may decrease with decreasing implant stability (Al-Jetaily & Al-Dosari 2011).

2.2.1 Bone structure

Cortical and trabecular parts of alveolar bone can be differentiated macroscopically. These two compartments may differ greatly in composition and density due to human anatomy and patient health status (Lekholm & Zarb 1985; Bayarchimeg et al. 2013; Gehrke et al. 2019). A prediction of success based solely on the bone structure therefore seems not to be possible (Dias et al. 2016). To a certain extent, irritation of bone can positively contribute to bone healing, due to the release of growth factors (Sotto-Maior et al. 2010; Cha et al. 2015; Baldi 2018). Nevertheless, in order not to jeopardize osseointegration, excessive bone damage during implant insertion (Cha et al. 2015) and especially micromotions exceeding 50-150 μm between implant and bone must be avoided (Dorogoy et al. 2017; Baldi et al. 2018) to prevent fibrous tissue formation (Yang et al. 2020). Generating high stress values to achieve primary implant stability, especially on cortical bone, can lead to disturbed stimulation of osteoblasts or even cell necrosis (Frisardi et al. 2012; Cha et al. 2015). Moreover, Trisi et al. (2013) observed that soft bone with lower density differed in contrast to medium or high bone in correlation between different insertion torque values and micromotion. A proportional correlation between increasing insertion torque and decreasing micromovement was observed only in medium or hard bone. Only soft bone showed values of micromotion above the dangerous threshold of 100 μm during an insertion torque of 20-35 Ncm (Trisi et al. 2013). This is supported by a study conducted by Nicolielo et al. (2020) pointing out that implant survival is best observed in intermediate bone types. On the other hand, a clinical study found that the microstructural bone characteristics did not affect remodeling of the marginal bone level and implant stability (Dias et al. 2016).

This example indicates that in some cases different, even contradictory results are met when comparing studies and thus there is a need for further research. Despite the partly contradictory findings presented, it can be assumed that a compromised osteotomy can negatively affect the healing and osseointegration of implants.

2.2.2 Implant design

A large variety of implant macrodesigns is available with manufactures making different claims with respect to their individual designs, aiming to optimize treatment protocols to work fast and effective for reaching implant stability (Dard et al. 2016; Pérez-Pevida et al. 2020). Various shapes are available, for example tapered or straight walled implants, which may differ in varying bone deformation (Steiner et al. 2020). Menicucci et al. (2012) showed that tapered implants exhibited better primary implant stability regardless of bone type in contrast to straight walled implants. Li Manni et al. (2020) investigated whether implants with triangular cross-sections placed in round osteotomies would relieve the buccal bone site and minimize bone loss, but could not find significant differences in comparison with round designs after one year. Furthermore, it has been shown that surface roughness, for example due to machining or acid etching (Dos Santos et al. 2011), also influences the extent of microdamage. In implants with treated surfaces, higher insertion torque values and higher implant stability quotients were observed in comparison to machined implants (Dos Santos et al. 2011). A rough cylindrical implant exhibited more microdamaged bone than a rough tapered or smooth implant (Bartold et al. 2011). In addition to the implant micro- and macrodesign, diameter and length of the implant must also be adapted to the situation, as larger diameters lead to a higher number of cracks (Taing-Watson et al. 2015). Short implants with a length of less than 8 mm have a higher risk of failure (Lemos et al. 2016).

2.2.3 Surgical procedure

In addition to bone quality and implant design, attention must also be paid to the surgical procedure. Basically, a distinction can be made between bone-specific and implant-specific drilling protocols (Elias et al. 2012; Taing-Watson et al. 2015; Dard et al. 2016; Fanali et al. 2021).

High insertion torque correlates with primary implant stability (Trisi et al. 2011) but also with a higher risk of harming the implant-abutment interface (Karl et al. 2017). In addition, higher compressive and tensile stress values on cortical and trabecular bone surrounding the implant are generated (Sotto-Maior et al. 2010), what ultimately can lead to bone loss (Duyck et al. 2010). The selection of conical implants is recommended for lower bone density, as higher insertion torque and higher compression in the cortical bone provide better stability (Aleo et al. 2012; Gehrke et al. 2019). An in vitro experiment compared implants with different macrodesigns and demonstrated that an increase in bone density basically led to an increase in insertion torque without changing the stability quotient (Gehrke et al. 2019). However, the individual macrodesigns presented differences in the insertion torque without affecting the implant stability quotient values.

A reduction of the insertion torque and thus a lower primary implant stability can only be discussed if an unloaded and protected healing of the implant is ensured (Lee et al. 2019). In general, insertion torques below 50 Ncm have been judged to be sufficient to achieve primary implant stability without compromising bone healing (Barone et al. 2016).

Another positive effect to prevent bone damage but simultaneously achieve a sufficient primary implant stability is brought about when implants are placed in predrilled holes (Taing-Watson et al. 2015). Because it is difficult to assess bone quality, certain drilling protocols often target compression, particularly in the cortical bone, in order to achieve primary implant stability in a save manner (Tabassum et al. 2014; Pérez-Pevida et al. 2020). Due to this fact, undersized drilling is one possibility the surgeon can adapt to a given situation to achieve an adequate degree of primary implant stability (Tabassum et al. 2010). However, excessive undersizing like a discrepancy of more than 15% between implant and final drill diameter must be avoided to prevent peri-implant stress (Tabassum et al. 2011). This applies in particular to cortical bone due to its lower viscoelasticity (Frisardi et al. 2012; Eom et al. 2016; Ikar et al. 2020). Otherwise it would lead to pronounced remodeling (Abrahamsson et al. 2021) or potentially bone necrosis (Coyac et al. 2019).

2.3 Secondary implant stability

Excessive bone damage during implant insertion must be avoided in order to achieve successful long term osseointegration. Secondary implant stability is ultimately achieved when bone remodeling and healing are completed (Dorogoy et al. 2017). It is the result of bone response to all influences at the time of implant insertion as well as during function (Albrektsson et al. 2017). This includes the abutment design (Agustín-Panadero et al. 2019; Palombo et al. 2021) and occlusal forces. Success in implant dentistry relates to esthetics and maintaince of hard and soft tissue. Initial marginal bone level changes between surgery and loading should later reach a steady state. Minor bone loss is commonly accepted in the range of < 1 mm in the first year after implant insertion and < 0,2 mm every following year (Eom et al. 2016; Ikar et al. 2020). In a recent study, marginal bone loss was reported to average 0.41 mm in 22 compared implant samples (Friberg & Ahmadzai 2019). Nevertheless, higher bone loss must be avoided at all costs, otherwise esthetic degradation, difficulties in cleaning the exposed implant surfaces and the risk of implant fracture may occur.

2.4 Objective of the present work

The factors described above may contribute to implant success or cause implant failure. Of great interest now would be the mutual interaction of the various factors. The aim of the present work is to study two current bone-level implant types with different configurations. Strain development during implant insertion and primary implant stability were analyzed to find any potential correlations with the histologically assessed bone damage. Furthermore, these implant types are compared with each other with regard to the above-mentioned parameters.

3 Material and Methods

3.1 Preliminary study

Different analyzing techniques were screened using a parametric study design to find out the most suitable techniques for the preparation of the samples. The following aspects were investigated:

- Leave implant in place after insertion or remove the implant
- Different embedding processes
- Various periods of time for resin infiltration under vacuum
- No staining, fuchsin or fluorescent dye

Bovine ribs (cool storage, untreated) were cut into twelve 30 mm cubes using a diamond band saw (EXAKT 300, EXAKT Advanced Technologies GmbH, Norderstedt, Germany). Afterwards, twelve tapered implants (Dr. Ihde STO 4.1×11 mm, Dr. Ihde Dental GmbH, Eching, Germany) were placed into predrilled sites (2,0 mm; 2,8 mm) in the centre of the samples using a surgical motor (iChiropro, BienAir, Biel, Switzerland) according to the manufacturer´s guidelines. For this purpose, a constant insertion speed of 25 rpm was selected during the entire implantation process and monitored using a surgical motor with digital transmission of the measurement parameters (iChiropro, BienAir, Biel, Switzerland). After implant insertion, implant stability was determined in two directions using resonance frequency analysis (Osstell ISQ device, Osstell AB, Gothenburg, Sweden).

In the following diagrams, the specimens are listed with their individual characteristics (Table 1) as well as the steps of the embedding process with the corresponding materials and concentrations (see appendix Table 7).

Table 1. *Overview of the various characteristics of the specimens 1-12*

Specimen	Implant	Infiltration	Staining
1	Insertion and removal	1 day Technovit® 9100*	Fuchsin**
2	Insertion and removal	3 days Technovit® 9100	Fuchsin
3	Insertion and removal	6 days Technovit® 9100	Fuchsin
4	Insertion	1 day Technovit® 9100	Fuchsin
5	Insertion	3 days Technovit® 9100	Fuchsin
6	Insertion	6 days Technovit® 9100	Fuchsin
7	Insertion	3 days Technovit® 9100	Fluorescent dye***
8	Insertion and removal	3 days Technovit® 9100	Fluorescent dye
9	Insertion	ProBase® ****	Fuchsin
10	Insertion	1 day Technovit® 9100	Fuchsin
11	Insertion	1 day Technovit® 9100	Fuchsin
12	Insertion	1 day Technovit® 9100	Fuchsin

* Technovit® 9100; Heraeus Kulzer, Hanau, Germany; ** Fuchsin, Resolab®, Bad Oeynhausen, Germany; *** MET-L-CHEK® Penetrant FP 97 A (M), Helling, Heidgraben, Germany; **** cold-curing polymer, ProBase®, Ivoclar Vivadent, Schaan, Liechtenstein

The samples were classified according to the factors mentioned above (Table 1, see appendix Table 7).

The samples were dehydrated in an ascending series of alcohol solutions of 70%, 80%, 90%, 96%, 99% diluted with distilled water (99 % Ethanol denatured; SAV Liquid Production GmbH, Flintsbach am Inn, Germany). The dehydration steps were carried out every second day. In addition, the process took place under vacuum and with a constant compression of 25 mmHg using a vacuum chamber (BACOENG® 1 Gallon Flat Stainless Steel Vacuum and Degassing Chamber, Suzhou Jianli Machinery And Equipment Co., LTD, Suzhou, China).

Specimen 9 was directly embedded in a cold-curing polymer (ProBase®; Ivoclar Vivadent, Schaan, Liechtenstein). All other samples followed the embedding protocol of a polymethylmethacrylate (Technovit® 9100; Heraeus Kulzer, Hanau, Germany) by additionally using a vacuum chamber. The final polymerisation took place in a refrigerator (4 °C) where all samples were stored in embedding moulds under anaerobic conditions.

After seven days, the samples were removed from the moulds and cut into 15 mm cubes. For microscopic inspection (LEICA DM4B; LEICA Mikrosysteme Vertrieb GmbH, Wetzlar, Germany), the specimens were prepared according to the sawing and grinding technique (Donath & Breuner 1982).

3.2 Main study

3.2.1 Implant systems

Two commercially available bone-level implant systems differing in macrodesign were selected. Astra implants represented a cylindric body with cervical microthreads while Straumann implants were parallel walled and showed a tapered apex (Table 2).

Table 2. *Dental Implant systems used and their corresponding drilling protocols*

	Straumann	**Astra**
Implant	Straumann Bone Level Tapered 4.1 × 12 mm (Institut Straumann AG, Basel, Switzerland)	OsseoSpeed TX 4.0 S × 13 mm (Astra Tech Implant System, Dentsply Implants Manufacturing GmbH, Mannheim, Germany)
Drill protocols	Needle drill 2.2 mm pilot drill 2.8 mm BLT drill 3.5 mm BLT drill	Round bur Twist drill 2.0 Twist drill 3.2 Twist drill 3.7

According to Klär et al. 2022

3.2.2 Implant insertion and biomechanical measurements

In order to reduce artefacts from repeated freezing and thawing of bone, the following steps were performed in one day.

Using the aboved mentioned diamond band saw, freshly acquired bovine ribs were cut into pieces with a diameter of 30 mm. In order to stabilize the specimens, metal holders and polyurethane resin (Biresin® G27; Sika Deutschland GmbH, Bad Urach, Germany) were used to fix them in an appropriate position. The samples were then randomly split into two groups (n = 5). Subsequently, pilot holes were drilled on the bone ridge using the surgical motor simulating clinical conditions. Axial osteotomy was performed with the aid of a metal guide. Furthermore, the manufacturer's drilling protocols for medium type bones were followed for all specimens (Table 2).

Using a dentin bonding agent (Syntac® Primer, Syntac® Adhesive, Heliobond®; Ivoclar Vivadent, Schaan, Liechtenstein) unidirectional strain gauges (LY11-0.6/120, 120Ω reference resistance; Hottinger Baldwin Messtechnik GmbH, Darmstadt, Germany) were placed on the buccal bone surface with the sensing element aligned in the mesio-distal direction (Grobecker-Karl et al. 2021). The corresponding solder tags (LS 7; Hottinger Baldwin Messtechnik GmbH, Darmstadt, Germany) were placed on the metal holders using cyanoacrylate as bonding system and followed by usual wiring to achieve a Wheatstone bridge. Finally, the implants were placed at a velocity of 25 rpm.
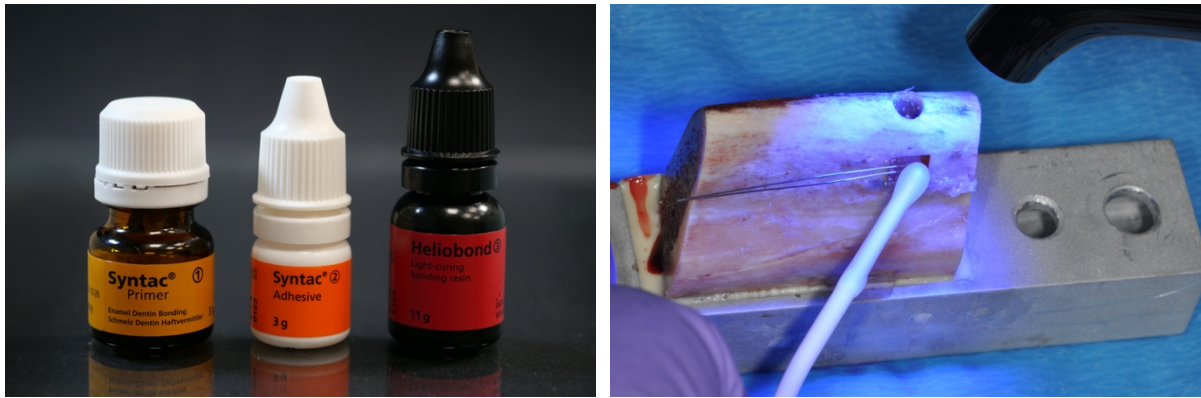
Figure 1. *Use of a dentin bonding agent to attach a unidirectional strain gauge on bone*

With the aid of a measurement amplifier (Quantum X; Hottinger Baldwin Messtechnik GmbH, Darmstadt, Germany) and analyzing software (jBEAM; AMS GmbH, Chemnitz, Germany), it was possible to measure strain development during implant insertion. As a final step, implant stability was determined by resonance frequency analysis (Osstell ISQ device; Osstell AB, Gothenburg, Sweden) in bucco-lingual and mesio-distal directions using implant specific smart peg abutments.
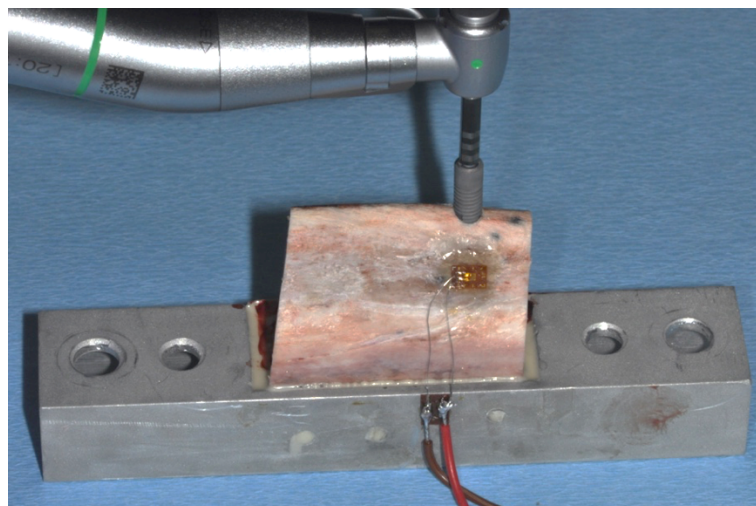
Figure 2. *Implant insertion in a bovine rib; a unidirectional strain gauge is fixed on the buccal bone surface*

3.2.3 Preparation of samples

After removing the strain gauges and metal holders, the specimens were cut with a distance of 10 mm to the implant surface using the diamond band saw. The optimal procedure derived from the preliminary study (see chapter 4.1) was applied. Therefore, every step was carried out using a vacuum chamber and a constant pressure of 25 mmHg (Table 3). Dehydration with ethanol lasted two days, and the total infiltration process lasted 6 days. To prepare the samples for the sawing and grinding technique described by Donath and Breuner (1982) after complete polymerisation of the resin, the diamond band saw was used to cut the specimens in the bucco-lingual direction, parallel to the axis and center of the implant and vertical to the center of the previously removed strain gauge.
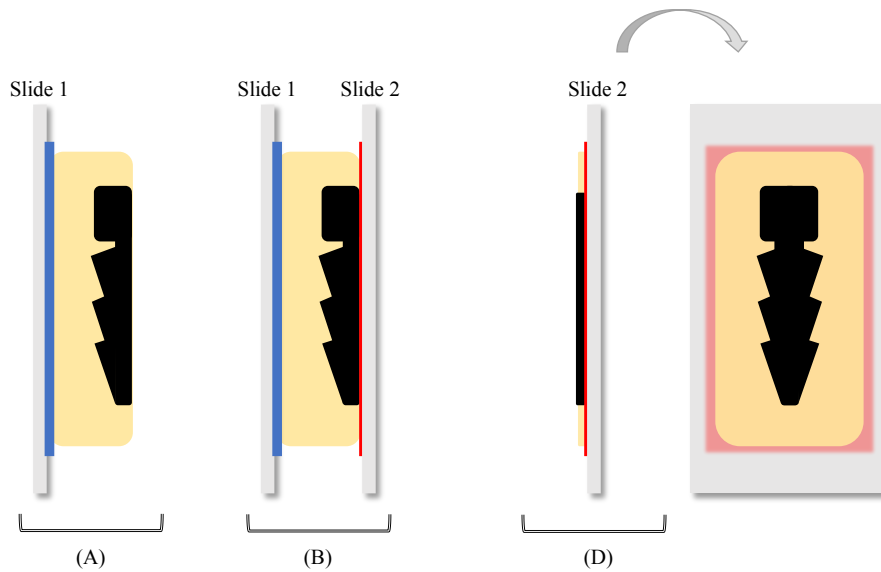
Figure 3. *Schematic illustration of the preparation of a histological section of an implant embedded in resin; cold curing polymer (blue); adhesive layer of a single-component precision adhesive (red) = [(B) – (slide 2) – (A)]; layer thickness of the specimen = [(D) – ((slide 2) + C)]*

First, a slide was roughened with a silicon carbid abrasive paper (WS FLEX 18 C P 320 grit sandpaper, Hermes Schleifmittel GmbH, Hamburg, Germany) and its thickness was measured (slide 1). Every thickness measurement was carried out using an electronic digital micrometer. The back of the specimen was coated with cold-curing resin (Technovit® 4000, Heraeus Kulzer, Hanau, Germany) (blue), placed on the previously roughened slide and cured in a precision adhesive press (EXAKT Advanced Technologies GmbH, Norderstedt, Germany) for 15 minutes under UV light. As a result, the specimen surface was nearly parallel to slide 1. A correction of irregularities as well as a rough polishing of the specimen was performed using a grinding machine (Grinding system TegraPol- 31, Struers ApS, Ballerup, Denmark) and silicon carbid abrasive papers (800, 1200 grit sandpaper). A triple measurement of the layer thickness between slide 1, Technovit® 4000 and the specimen was noted and a mean value calculated (A). A new polished slide (slide 2) was measured and its thickness was noted. For precision bonding, a light-curing single-component precision adhesive (Technovit® 7210 VLC, Heraeus Kulzer, Hanau, Germany) was applied centrally to the implant (red), pressed against slide 2 in the precision adhesive press and cured for 15 minutes under UV light. This was followed by a triple measurement in the area of the implant (B). Using the diamond band saw, thin sections were produced and reduced to a layer thickness of approximately 200 μm using the grinding machine (D). The layer thickness was determined according to the following formula:

Adhesive layer C (red) = [(B) – (slide 2) – (A)]

Layer thickness of the specimen = [(D) – ((slide 2) + C)]

With a thickness of 120 μm, microradiographs (Faxitron X-ray, Lincolnshire, IL, USA; 14 kV, 0.3 mA, 2.5 min; Insight Dental Film, Carestream Health Inc., Rochester, NY, USA) of the specimens were obtained to determine the bone density of the regions of interest. To evaluate the samples histomorphometrically, it was necessary to reduce them to a final thickness of approximately 30 μm prior to polishing the specimens using the grinding machine (1200, 2500 and 4000 grit sandpaper).

Table 3. Embedding protocol for the final experimental setup

Step	Process under vacuum	Materials	Concentration/ ratio	Time in days
1	Dehydration	Ethanol 99% denatured	70%	1
2	"	"	70%	1
3	"	"	80%	1
4	"	"	80%	1
5	"	"	90%	1
6	"	"	90%	1
7	"	"	96%	1
8	"	"	96%	1
9	"	"	100%	1
10	"	"	100%	1
11	Rinsing	Ethanol 99% denatured	100%	6
12	Intermedium	Xylene	100%	1
13	Preinfiltration I	Technovit® 9100 stabilised Xylene	1:1	1
14	Preinfiltration II	Technovit® 9100 stabilised Technovit® 9100 hardener 1	200 ml 1g	6
15	Preinfiltration III	Technovit® 9100 destabilised Technovit® 9100 hardener 1	200 ml 1g	6
16	Infiltration	Technovit® 9100 destabilised Technovit® 9100 hardener 1 Technovit® 9100 PMMA-powder	250 ml 1g 20 g	6
17	Polymerisation	Technovit® 9100 stock solution A Technovit® 9100 stock solution B	9A:1B	6

3.2.4 Histologic evaluation

By analyzing the microradiographs, bone mineral density (BMD) was measured with the aid of a color image analyzing system (LEICA Application Suite, LEICA Phase Expert; LEICA Mikrosysteme Vertrieb GmbH, Wetzlar, Germany). To this end, each sample was divided into four parts: cortical left, trabecular left, cortical right, trabecular right. A reference surface in the cortical region was used to identify the bone. Subsequently, bone mineral density could be measured along the implant surface based on the gray scale of the reference surface. Especially in cancellous bone, non-bone components such as impurities created during preparation showed similar gray values. These were localized using the microscope and manually removed from the measurement so as not to falsify BMD.

(a)   (b)
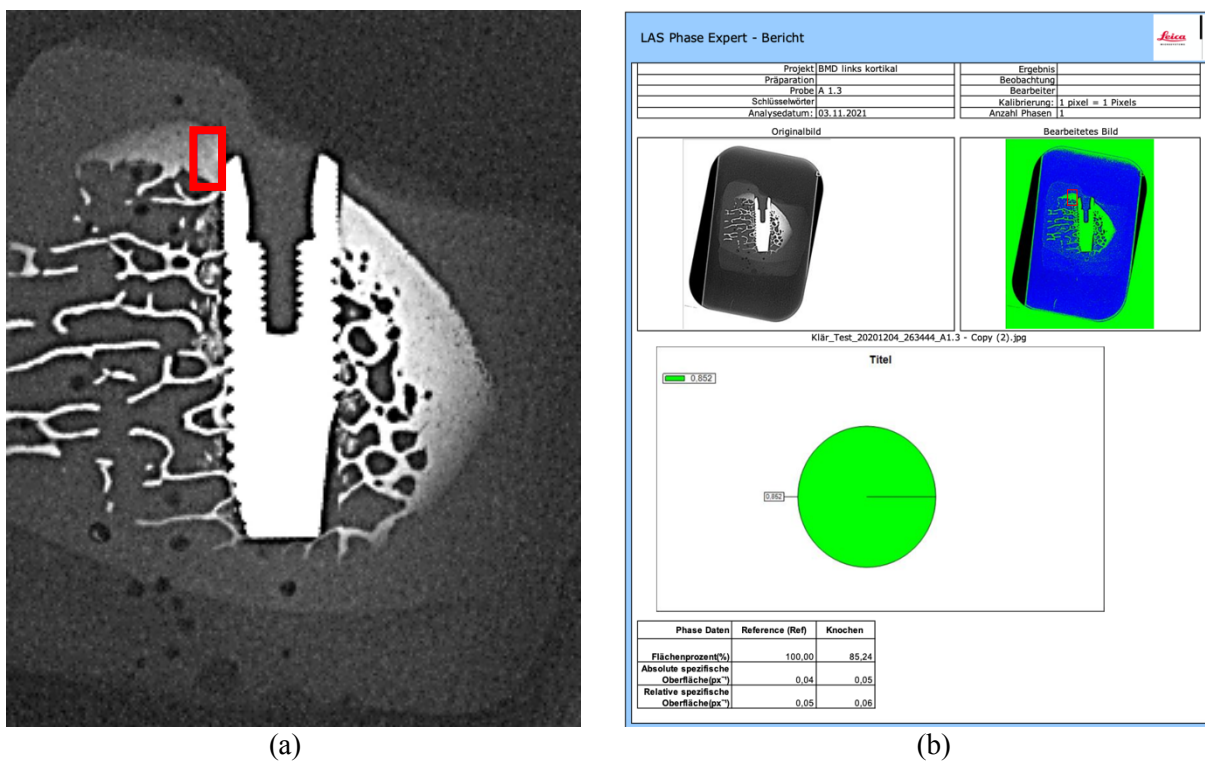
Figure 4. *(a) Example of a microradiograph (specimen A 1.3) to evaluate bone mineral density (BMD): Definition of a region of interest ROI = left cortical; (b) Extract from the Phase Expert report; the same subdivision was also made for left trabecular, right cortical and right trabecular bone areas*
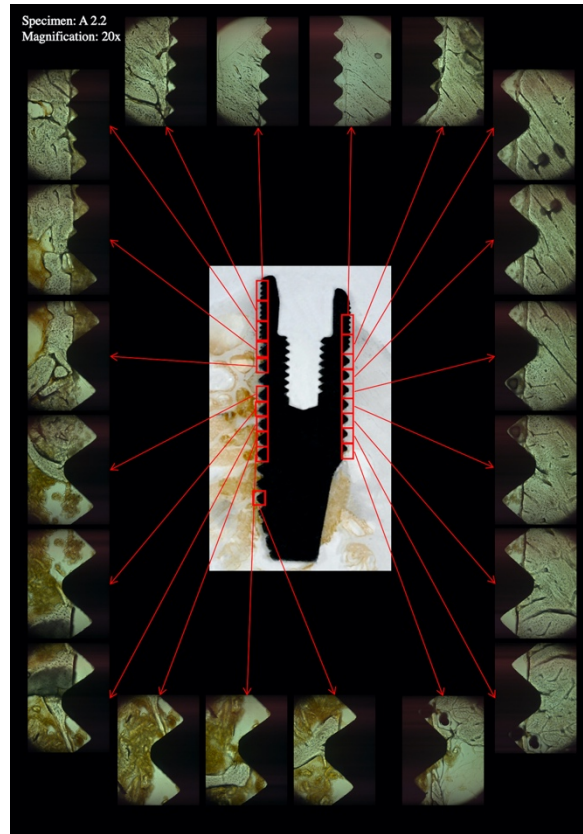
Figure 5. *Overview of an OsseoSpeed implant placed in a bovine rib with corresponding histologic images at 20x magnification*
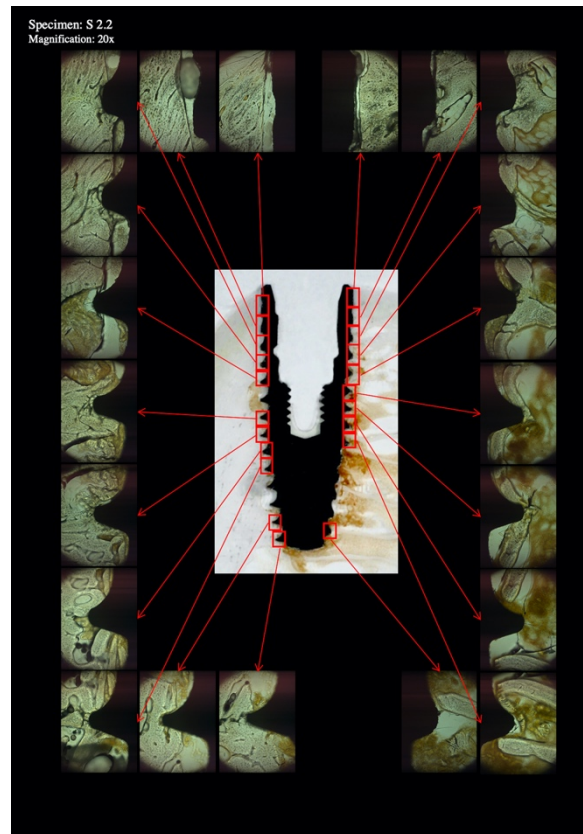
Figure 6. *Overview of a Straumann BLT implant placed in a bovine rib with corresponding histologic images at 20x magnification*

At a magnification of 20x the samples were examined histomorphometrically under the above-mentioned microscope in combination with the color image analyzing system.

As a first step, BIC was defined as the bone to implant contact (Figure 7). For this purpose, circles with a diameter of 500 μm (yellow circle) from the implant surface (yellow line) were drawn. The inner corner of the osteotomy within this radius was defined as BIC (red line) (Tabassum et al. 2014). The length of the measured relevant bone surface divided by the length of the implant surface led to the percentage of BIC. In the second step, the region of interest was defined by creating radii of 300 μm (yellow circles; Figure 8) starting from the previously defined bone inner surface (red line). The region between the connection line (blue line) of the radii and the bony wall determined the region on interest.
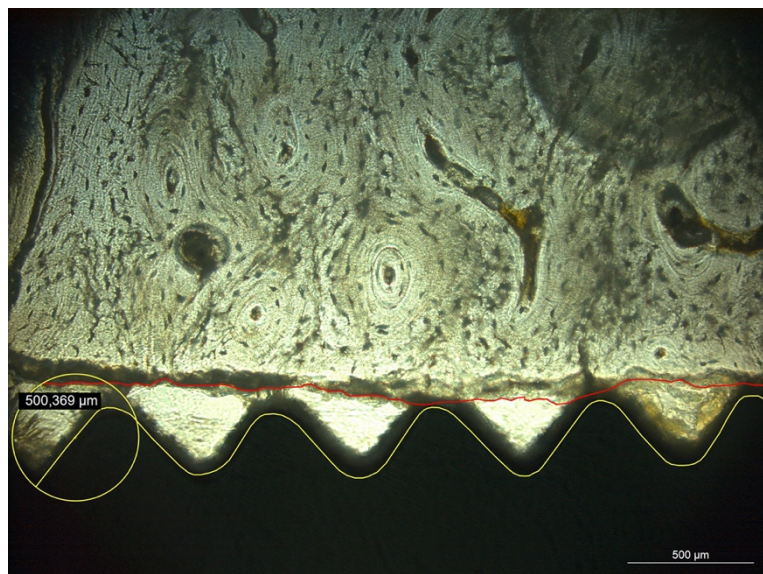
Figure 7. *Determination of bone to implant contact (BIC); implant surface (yellow line); bone wall (red line); circles with a diameter of 500 μm (yellow circle)*
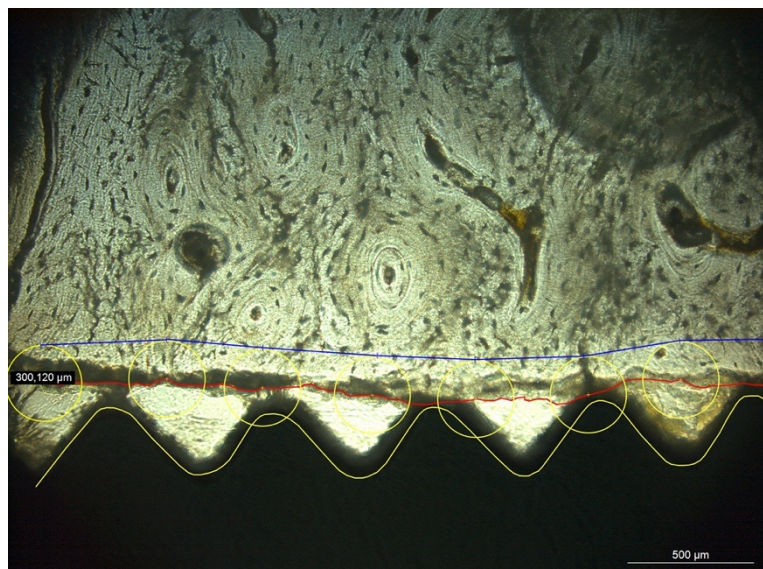
Figure 8. *Determination of the region of interest*

In this region, bone damage was recorded as deformed bone or as cracks, whereby cracks equal or greater than 100 µm were classified to be macrocracks and those less than 100 µm were classified as microcracks. By using the color analyzing system, bone damage was evaluated manually.

(a)

(b)

(c)

Figure 9. *(a) Example of deformed bone in the form of grouped stretch marks at the outermost point of the implant thread (Specimen A 4.3 R12); (b) Example of macrocracks surrounding the implant surface (Specimen S 2.2 R3); (c) Example of microcracks surrounding the implant surface (Specimen S 2.2 L10)*

3.2.5 Statistical analysis

According to the procedure described in chapter 3.2.2, maximum insertion torque and strain development on the buccal bone surface were measured during insertion, followed by the determination of implant stability. In addition, for histologic analysis cortical and cancellous components of bone were distinguished from each other. Under this aspect, bone mineral density, bone to implant contact, microcracks, macrocracks and deformed areas were also included in the statistical analysis.

For each implant type, mean values and standard deviations of the parameters mentioned were calculated. Following descriptive statistics, Shapiro-Wilk tests on normality of distribution of measurement values were performed, followed by Welch t-Tests for comparing Astra vs. Straumann implants (n = 5). Pearson product moment correlation coefficients were calculated for evaluating potential correlations among measurement parameters. All calculations were performed with the R software package (R, The R Foundation for Statistical Computing, Vienna, Austria; www.R-project.org; accessed 18 November 2021).

For all comparisons, the level of significance was set at $\alpha = 0.05$.

4 Results

4.1 Preliminary study

4.1.1 Implant removal

First, a decision has to be made whether the implant should remain in place or be removed concerning the assessment of damage as well as bone to implant contact. Microscopic examination revealed that the thread was clearly defined when leaving the implant in place whereas removing the implant appeared to obliterate it. Moreover, there was a risk of generating more bone damage by removing the implant. This led to the decision to leave the implant in place.
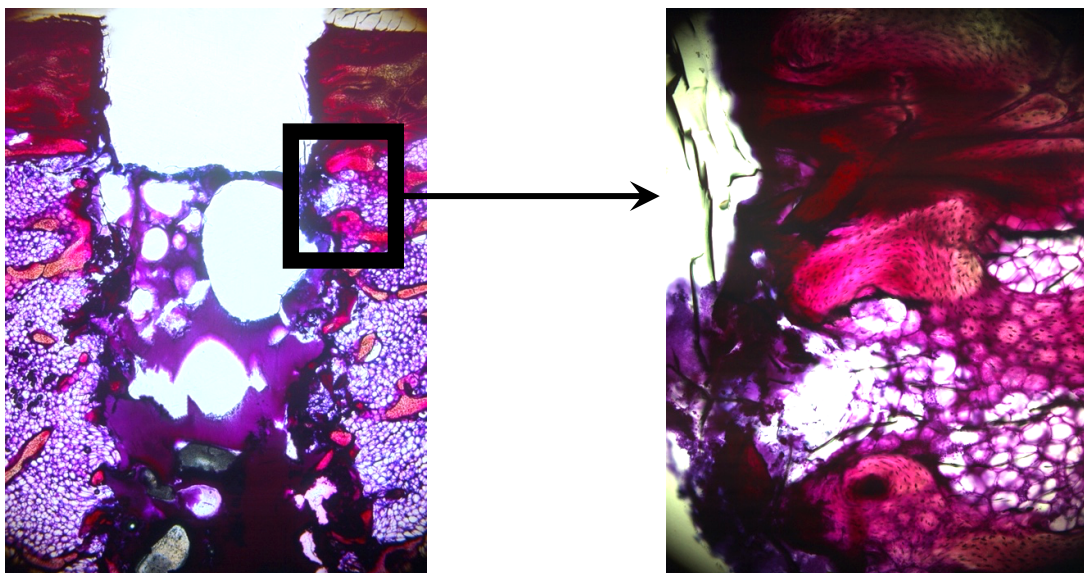
Specimen 2: Overview (magnification 2,5x) and detail (magnification 10x)
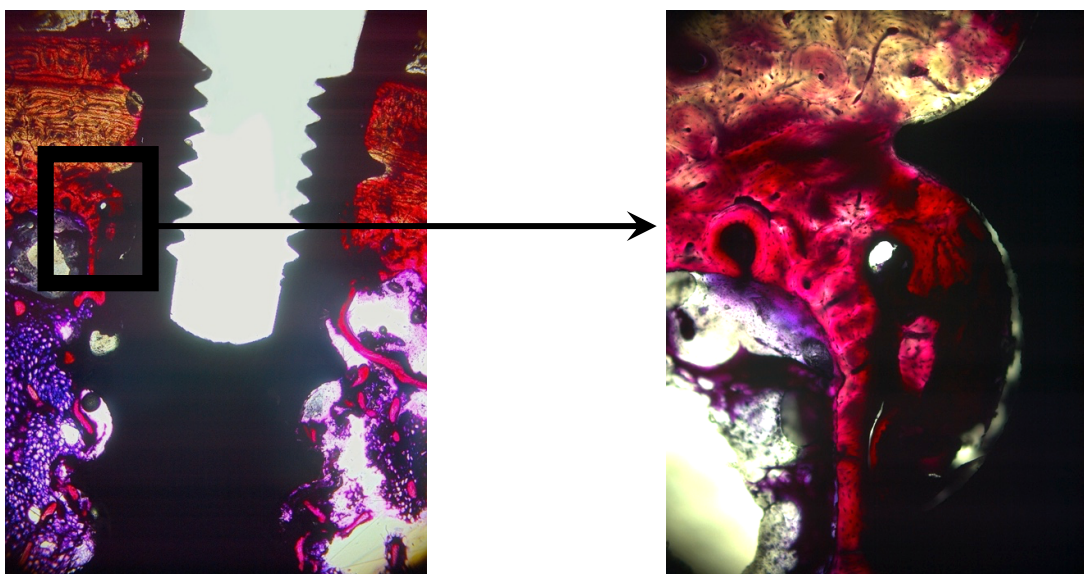
Specimen 5: Overview (magnification 2,5x) and detail (magnification 10x)

Figure 10. *Comparing sites with implant removed vs. sites with implant in place; Specimen 2 - adequate observation of the defining thread not possible; Specimen 5 - the thread is clearly observable*

4.1.2 Resin infiltration

The selection of embedding materials referred to two different resins: a standard histologic resin (Technovit® 9100) vs. a cold curing denture resin (ProBase®). Extreme shrinkage during polymerisation of ProBase® (specimen 9) caused stresses and consequently cracking within the cold curing polymer so that this could have falsified the evaluation. At least under macroscopic observation, the specimens embedded in Technovit® 9100 showed satisfying results with respect to material application, polymerisation and grinding.

4.1.3 Infiltration period

The basic concept was to optimize bone penetration and accelerate the embedding process by using a vacuum chamber and a consistent pressure of 25 mmHg. Different times of infiltration (Table 1) revealed a macroscopically as well as microscopically recognizable difference between the samples. The specimens with the shorter infiltration time (one day vs. three days) exhibited considerably more inclusion of air as well as non-homogeneous resin infiltration. The samples with the longest time of infiltration delivered optimal results, so that the decision was made to keep the respective infiltration steps with Technovit® 9100 under vacuum for six days.

Figure 11. *Macroscopic comparison of specimens with different times of infiltration; left specimen 10.3, middle specimen 5.3, right specimen 6.2; from left to right, an increase in the homogeneity of the resin infiltration can be observed*

4.1.4 Staining

Fuchsin as well as fluorescent dye were used during the embedding process. Microscopic examination of the specimen stained with fuchsin revealed both nonuniform staining and color oversaturation. On the other hand, fluorescent staining showed partially weak contrast ratios and uneven exposure. Therefore, in both cases, identification of bone damage was not feasible. Observation of specimen 7 and 8 under natural light showed even illustration and strong contrasts. Thus, the samples were not stained in the main experiment.

(a)   (b)
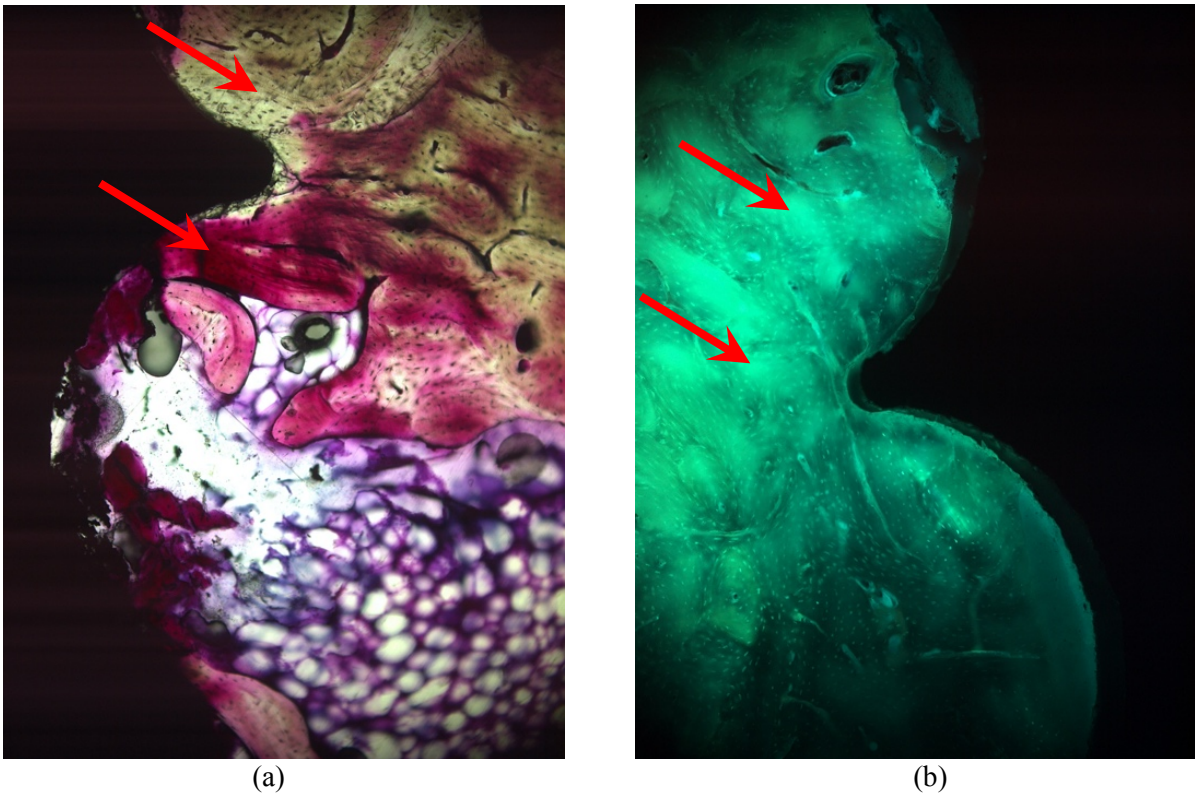
Figure 12. *(a) Specimen 6.3: uneven staining and partial oversaturation of fuchsin; (b) Specimen 7.2: uncontrolled exposure and partially weak contrasts*

4.2 Main study

4.2.1 Descriptive and comparative statistics

The mean values as well as the standard deviations of the considered parameters for the two implant systems are shown in Table 4. Based on the Shapiro-Wilk tests, in five instances, a non-normal distribution of measurement values was indicated.

In comparison, insertion torque (p = 0.772), strain development (p = 0.893) and implant stability (p = 0.642) were slightly higher in Straumann implants. Bone to implant contact in cortical bone (p = 0.466) as well as trabecular bone (p = 0.360) did not differ between the two implant types.

In three cases, the Welch *t*-Tests showed a significant difference between the two implant systems used. Straumann showed significantly higher values of BICc (p = 0.014) and BICt (p = 0.016) while Astra showed significantly greater values of microcracks in cortical bone (p = 0.020).

The number of microcracks in trabecular bone (p = 0.969) was in Straumann specimens somewhat higher than in Astra, as well as the number of macrocracks in cortical bone (p = 0.893) and trabecular bone (p = 0.600). Astra showed greater deformed bone areas in the cortical region (p = 0.320), whereas Straumann implants revealed greater deformed bone areas in the trabecular region (p = 0.699).

Table 4. *Descriptive statistics and pairwise comparisons of the two implant types investigated*

	Astra		Straumann		Welch *t*-Tests (p-value)
	Mean	SD	Mean	SD	
Torque	29.76	26.893	34.08	17.428	0.772
Strain	383.38	299.860	410.84	284.754	0.893
ISQ	* 79.20	11.339	81.80	2.842	0.642
BMDc	0.894	0.025	0.872	0.058	0.466
BMDt	0.486	0.099	0.434	0.065	0.360
BICc	0.756	0.059	0.868	0.054	**0.014**
BICt	0.428	0.064	0.600	0.101	**0.016**
microC	** 92.204	26.241	49.732	7.318	**0.020**
microT	*** 44.484	18.810	**** 45.034	23.733	0.969
macroC	10.862	1.443	11.020	2.073	0.893
macroT	5.494	0.976	6.286	3.045	0.600
defC	0.592	0.504	0.326	0.195	0.320
defT	0.368	0.161	***** 0.418	0.226	0.699

*Significant differences between the groups (p < 0.05) are written in bold; p-values of Shapiro-Wilk tests showing a non-normal distribution of measured values: * 0.014; ** 0.019; *** 0.050; **** 0.028; ***** 0.004; according to Klär et al. 2022*

4.2.2 Correlations between parameters

Astra implants

The correlation coefficients as well as the p-values of the Astra group are given in Table 5. Within this group, three significant correlations were found. Higher insertion torque led to increased bone to implant contact in trabecular bone ($p = 0.007$). In cortical bone, greater bone to implant contact led to higher numbers of macrocracks ($p = 0.019$). Higher implant stability correlated with a higher number of macrocracks in trabecular bone ($p = 0.016$).

Straumann implants

The correlation coefficients as well as the p-values of the Straumann group are given in Table 6. Within this group, two significant correlations were found. Higher insertion torque led to lower bone to implant contact in cortical bone ($p = 0.029$) and higher bone to implant contact trabecular correlated with an increased number of macrocracks in trabecular bone ($p = 0.029$).

***Table 5.** Correlation coefficients and p-values of the Astra group*

	Torque	Strain	ISQ	BMDc	BMDt	BICc	BICt	microC	microT	macroC	macroT	defC	defT
											Correlation Coefficients		
Torque		−0.239	0.665	0.635	0.867	−0.431	0.969	−0.259	−0.212	−0.502	0.726	0.179	0.549
Strain	0.761		0.511	0.443	0.300	0.859	0.013	0.861	0.745	0.870	−0.700	−0.566	−0.902
ISQ	0.221	0.490		0.664	0.762	0.003	0.665	0.093	0.393	0.107	0.943	0.313	0.006
BMDc	0.250	0.557	0.222		0.652	0.385	0.782	−0.007	0.003	0.220	0.503	0.339	−0.115
BMDt	0.057	0.700	0.134	0.233		−0.128	0.896	0.251	0.270	−0.105	0.685	−0.173	0.119
BICc	0.469	0.141	0.996	0.522	0.838		−0.207	0.559	0.459	0.937	−0.305	−0.095	−0.911
BICt	**0.007**	0.987	0.220	0.118	0.039	0.738		−0.140	−0.152	−0.320	0.650	0.135	0.369
microC	0.674	0.140	0.882	0.992	0.684	0.327	0.823		0.885	0.721	−0.171	−0.773	−0.809
microT	0.732	0.255	0.513	0.997	0.660	0.437	0.807	0.046		0.718	0.180	−0.485	−0.743
macroC	0.329	0.130	0.864	0.722	0.867	**0.019**	0.599	0.169	0.172		−0.194	−0.200	−0.983
macroT	0.165	0.230	**0.016**	0.388	0.202	0.618	0.236	0.783	0.772	0.755		0.439	0.310
defC	0.774	0.434	0.609	0.577	0.780	0.879	0.828	0.125	0.408	0.746	0.460		0.370
defT	0.338	0.098	0.993	0.854	0.849	0.032	0.541	0.098	0.150	0.003	0.612	0.540	
p-values													

Significant p-values are written in bold (p < 0.05); according to Klär et al. 2022

Table 6. Correlation coefficients and p-values of the Straumann group

												Correlation Coefficients	
	Torque	**Strain**	**ISQ**	**BMDc**	**BMDt**	**BICc**	**BICt**	**microC**	**microT**	**macroC**	**macroT**	**defC**	**defT**
Torque		−0.138	0.040	0.120	0.237	−0.916	0.458	−0.308	0.483	0.498	0.681	−0.036	−0.764
Strain	0.825		0.023	0.624	0.578	0.351	−0.560	−0.235	−0.164	−0.048	−0.252	0.673	−0.480
ISQ	0.949	0.970		0.362	0.335	0.301	−0.600	0.618	−0.819	0.608	−0.597	0.699	−0.115
BMDc	0.848	0.261	0.550		0.992	0.156	−0.754	0.434	−0.127	0.701	−0.472	0.852	−0.327
BMDt	0.701	0.307	0.582	0.001		0.031	−0.672	0.394	−0.039	0.748	−0.372	0.810	−0.394
BICc	**0.029**	0.562	0.623	0.803	0.960		−0.737	0.435	−0.739	−0.251	−0.868	0.415	0.545
BICt	0.438	0.326	0.285	0.141	0.214	0.155		−0.656	0.676	−0.403	0.915	−0.884	−0.118
microC	0.615	0.703	0.266	0.466	0.512	0.464	0.230		−0.499	0.629	−0.791	0.440	0.520
microT	0.410	0.792	0.090	0.839	0.950	0.154	0.211	0.392		−0.100	0.777	−0.586	−0.139
macroC	0.394	0.939	0.277	0.187	0.146	0.684	0.502	0.255	0.873		−0.256	0.576	−0.272
macroT	0.206	0.682	0.288	0.423	0.537	0.056	**0.029**	0.111	0.122	0.677		−0.655	−0.473
defC	0.954	0.213	0.189	0.067	0.097	0.487	0.047	0.459	0.299	0.310	0.230		−0.346
defT	0.133	0.414	0.854	0.591	0.512	0.342	0.851	0.370	0.756	0.658	0.421	0.569	
	p-values												

Significant p-values are written in bold ($p < 0.05$); according to Klär et al. 2022

5 Discussion

In this in vitro study, two implant systems with their corresponding drilling protocols were used and inserted into bovine ribs. These implant systems differed in length, diameter and thread design. During implant insertion, strain development of the bone surrounding the implant was measured. Subsequently, bone damage was evaluated histologically as crack formation and deformed areas in bone. Descriptive and comparative analysis of insertion torque, strain development and implant stability quotient were performed with both implant types. Furthermore, bone mineral density (cortical and trabecular), bone to implant contact (cortical and trabecular), microcracks (cortical and trabecular), macrocracks (cortical and trabecular) and deformed areas (cortical and trabecular) were analyzed. In addition, the correlations between the mentioned parameters were examined. This biomechanical and histological examination served to find reasons for bone loss after implant insertion.

5.1 Findings

One main characteristic of successful implantation is achieving osseointegration after healing, meaning that bone has actively grown to the implant surface without any remodeling to fibrous connective tissue or even formation of dead spaces (Albrektsson & Johansson 2001; Misch et al 2008). In principle, it can be assumed that mechanical traumatization of bone can lead to bone resorption. Therefore, basic prerequisites are avoiding excessive bone damage during the surgical procedure as well as attaining primary implant stability immediately after insertion to avoid micromovements and to allow healing (Trisi et al. 2013; Cha et al. 2015; Dorogoy et al. 2017; Baldi et al. 2018). In order to achieve primary implant stability, implantologists have aimed to place implants with a high insertion torque as this leads to higher values of bone to implant contact. Especially for immediate loading of implants, clinicians often opt for a higher insertion torque, which supposedly suggests more secure and better osseointegration of the implant due to the higher primary stability values (Ikar et al. 2020). On the other hand, high insertion torque values (> 50 Ncm) have been reported to result in higher compressive stress values to peri-implant tissue, thus causing disturbed stimulation of osteoblasts, impaired blood supply and even bone necrosis (Sotto-Maior et al. 2010; Frisardi et al. 2012; Dorogoy et al. 2017). Consequently, this is not conducive to osseointegration, especially for immediate loading, because initial bone resorption can lead to micromotion and this can lead to even more resorption and connective tissue remodeling (Cha et al. 2015).

Due to different viscoelasticity, cortical bone is more likely to exhibit higher stress values, whereas trabecular bone rather exhibits higher strain values (Ikar et al. 2020). Especially with regard to esthetic and functional aspects, high stress development in cortical bone should be avoided. For example, this can be performed by using crestal drills. Strain in the trabecular bone is assumed to be less dangerous (Ikar et al. 2020).

In the present in vitro study, a tremendous impact on the surrounding bone, caused by the implementation of the correct drilling protocol as well as implant placement, was histologically demonstrated in both implant types. This mechanical trauma was observed in trabecular and cortical bone immediately surrounding the implants where enormous crack formations and deformed areas were found, even though the implants were inserted in pilot holes (Taing-Watson et al. 2015). Whether this would affect healing and thus secondary implant stability in an in vivo setting is difficult to assess, as thresholds for bone damage are still unknown and it is difficult to evaluate the extent to which bone irritation may accelerate or impair healing (Sotto-Maior et al. 2010, Cha et al. 2015, Baldi et al. 2018).

Depending on individual circumstances, the quality and quantity of bone is the most variable and difficult factor to predict in dental implantation (Gehrke et al. 2019; Bayarchimeg et al. 2013). For this reason, bone loss of < 1 mm in the first year after implant placement is nevertheless considered a successful therapy (Eom et al. 2016; Albrektsson et al. 2017; Friberg & Ahmadzai 2019; Ikar et al. 2020).

Fresh bovine ribs were used to simulate a jaw bone ridge. This may explain why large differences appeared in both the measurements and the analysis. The experimental bone material used had considerable differences in the thickness of the cortical bone. To minimize the effect of bone composition, a much greater sample size would have been required. However, this could not be implemented within the scope of this study. In addition, comparability with other studies is difficult because there is no uniform standardization of the experimental setup. Therefore, it would be reasonable to use foams as bone substitutes to establish comparability (Karl et al. 2018; Pérez-Pevida et al. 2020). However, the use of foam (Pérez-Pevida et al. 2020) and excessive undersizing of osteotomies (Abrahamsson et al. 2021) was omitted to best reflect clinical practice.

As already mentioned, the bone mineral density was not significantly different between the specimens. Accordingly, another factor must have been the reason for the stability of the two implant systems. This could, for example, be due to the dissimilar macrodesign resulting in varying bone to implant contact values (Dard et al. 2016; Gehrke et al. 2019). In terms of macrodesign and regardless of the bone type, the literature describes higher primary implant stability when using tapered implants (Menicucci et al. 2012). However, tapered implants result in more bone damage when compared to smooth cylindrical implants and less bone damage when compared to rough cylindrical implants (Bartold et al. 2011; Menicucci et al. 2012). This emphasizes the effect of the surface condition of implants on the surrounding bone. In this in vitro study, each implant was used only once, as the surface roughness may influence the insertion and bone damage. Ultimately, the comparison between the two implant systems used shows that the macrodesign of Straumann implants in combination with the drilling protocol used seems to result in less damage to the cortical bone in spite of its tapered macrodesign.

Because of differences in implant design and by following the manufacturer's instructions, the insertion process was accompanied by different initial positions in the vertical as well as different time requirements despite a uniform insertion speed of 25 rpm. Nevertheless, both implant systems with their individual macrodesign characteristics achieved sufficient primary implant stability in vitro with approximately equal values. According to Chen et al. (2019) this would clearly minimize the risk of implant loss for both implant types. With regard to bone damage, Astra implant samples exhibited significantly higher values for microcracks cortically, which may depend on the specific drilling protocol in combination with the implant design.

5.2 Experimental limitations

To determine the most appropriate technique for the preparation and analysis of the above-mentioned main samples, an independent preliminary test was performed with a third implant system and different analysis techniques. The advantages and disadvantages of removing or leaving the implant in place after insertion, diverse embedding materials, different periods of time under vacuum as well as various staining methods were investigated. The decision was made to leave the implant in place in order to maintain the exact definition of the thread of the implant and to subsequently evaluate the bone to implant contact as well as to avoid additional bone damage. The longest preparation time under vacuum (six days) led to best results in terms of uniformity of resin infiltration and avoiding air entrapment. In literature, the analysis of bone damage by staining with fuchsin is described (Burr & Hooser 1995). Due to the preliminary tests with different staining methods and the associated difficulties in assessing bone damage, cracking as well as bone deformation was evaluated in the main experiment in native bone.

All strain gauges remained in place during the surgical procedure (Grobecker-Karl 2021; Klär et al. 2022). The preparation of the specimens with polymethylmethacrylate (Technovit® 9100) and a vacuum chamber proceeded without complications as shown in the preliminary test. Both in the sawing and grinding technique and in polishing of the specimens, special emphasis was placed on careful and low-damage preparation. Additional damage to the bone could not be demonstrated, but also not completely excluded.

Bone to implant contact (BIC) describes a very close contact between dental implants and bone during as well as after healing. In this in vitro study, BIC was considered as an area of potential bone-implant interaction due to implant site preparation as well as implant placement. To this end, initial histologic observations of the specimens indicated that the bony wall within a 500 μm radius of the outermost point of the implant was to be considered BIC (Tabassum et al. 2014). Precisely defining the boundary of the region of interest proved to be difficult, because the effects of implant site preparation and implant insertion, different implant macrodesigns and differences in bone density on bone damage could only be assessed by initial review of histologic sections. On this basis, a range of 300 μm was considered appropriate for both implant types within which bone damage was assessed.

Bone damage was counted by hand three times in an unbiased way. During the evaluation, both macrocracks and deformed areas could be clearly identified. To avoid misinterpretations due to anatomical structures and impurities, only clearly definable cracks were included in the evaluation, especially when counting microcracks.

Correlations between the parameters were examined, which yielded few significant results. One reason for this could be a difficult comparability of the measured values. For example, the insertion torque and strain development have a circular effect on the implant and the surrounding bone, whereas in this case, the histological analysis focuses only on the implant center. Another reason could be the small number of samples. The Shapiro-Wilk test was chosen with a significance level of $p < 0.05$. Nevertheless, a normal distribution of the measured values could not be guaranteed due to the small number of specimens. Consequently, the Welch t-Tests for pairwise comparisons as well as the Pearson product moment correlation coefficients could be affected by any deviation in the normal distribution. Nonparametric tests therefore appeared to be unnecessary. Due to the small sample size, the statistical power was also low (< 0.8), except for the parameters BICt and microC. Non-significant differences can thus be interpreted as second-order errors, but significant measured values are not falsified by this.

5.3 Conclusion

Bone to implant contact in cortical as well as trabecular bone was significant higher in Straumann implant samples. However, higher insertion torque led to lower bone to implant contact cortical. Higher bone to implant contact trabecular led to an increased number of macrocracks in trabecular bone.

Astra implant samples showed significantly higher values for bone damage with regard to microcracks in the cortical bone area. Higher insertion torque correlated with a higher bone to implant contact in trabecular bone. Greater bone to implant contact cortical correlated with a higher number of macrocracks cortical, and in trabecular bone higher implant stability led to a higher number of macrocracks. Both implant systems achieved sufficient primary implant stability.

Bone damage of varying extent is to be expected when using current implant systems with their individual characteristics and specific drilling protocols. Undersizing of an osteotomy in relation to the implant diameter increases primary implant stability, but seems to be associated with an increased degree of bone damage. Implant macrodesign has a significant effect on the irritation of the bone during implant surgery. Within the limitations of this in vitro study it can be concluded that newly developed implant designs should increase stability in trabecular bone and minimize the loading of cortical bone. Overall, drilling protocols should be developed that provide for minimal removal of alveolar bone.

6 References

1. Abrahamsson I, Carcuac O, Berglundh T (2021) Influence of implant geometry and osteotomy design on early bone healing: A pre-clinical in vivo study. Clinical Oral Implants Research 32:1190-1199

2. Agustín-Panadero R, Martínez-Martínez N, Fernandez-Estevan L, Faus-López J, Solá-Ruíz MF (2019) Influence of Transmucosal Area Morphology on Peri-Implant Bone Loss in Tissue-Level Implants. The International Journal of Oral and Maxillofacial Implants 34:947-952

3. Al-Jetaily S, Al-Dosari AA (2011) Assessment of Osstell™ and Periotest® systems in measuring dental implant stability (in vitro study). The Saudi Dental Journal 23:17-21

4. Albrektsson T, Johansson C (2001) Osteoinduction, osteoconduction and osseointegration. European Spine Journal 10:96-101

5. Albrektsson T, Chrcanovic B, Östman PO, Sennerby L (2017) Initial and long-term crestal bone responses to modern dental implants. Periodontology 2000 73:41-50

6. Aleo E, Varvara G, Scarano A, Sinjari B, Murmura G (2012) Comparison of the primary stabilities of conical and cylindrical endosseous dental implants: an in-vitro study. Journal of Biological Regulators and Homeostatic Agents 26:89-96

7. Aparicio C (1997) The use of the Periotest value as the initial success criteria of an implant: 8-year report. The International Journal of Periodontics and Restorative Dentistry 17:150-161

8. Baldi D, Lombardi T, Colombo J, Cervino G, Perinetti G, Di Lenarda R, Stacchi C (2018) Correlation between Insertion Torque and Implant Stability Quotient in Tapered Implants with Knife-Edge Thread Design. BioMed Research International 2018:7201093

9. Barone A, Alfonsi F, Derchi G, Tonelli P, Toti P, Marchionni S, Covani U (2016) The Effect of Insertion Torque on the Clinical Outcome of Single Implants: A Randomized Clinical Trial. Clinical Implant Dentistry and Related Research 18:588-600

10. Bartold PM, Kuliwaba JS, Lee V, Shah S, Marino V, Fazzalari NL (2011) Influence of surface roughness and shape on microdamage of the osseous surface adjacent to titanium dental implants. Clinical Oral Implants Research 22:613-618

11. Bayarchimeg D, Namgoong H, Kim BK, Kim MD, Kim S, Kim TI, Seol YJ, Lee YM, Ku Y, Rhyu IC, Lee EH, Koo KT (2013) Evaluation of the correlation between insertion torque and primary stability of dental implants using a block bone test. Journal of Periodontal and Implant Science 43:30-36

12. Brånemark PI (1983) Osseointegration and its experimental background. The Journal of Prosthetic Dentistry 50:399-410

13. Burr DB, Hooser M (1995) Alterations to the en bloc basic fuchsin staining protocol for the demonstration of microdamage produced in vivo. Bone 17:431-433

14. Cha JY, Pereira MD, Smith AA, Houschyar KS, Yin X, Mouraret S, Brunski JB, Helms JA (2015) Multiscale analyses of the bone-implant interface. Journal of Dental Research 94:482-490

15. Chen MH, Lyons K, Tawse-Smith A, Ma S (2019) Resonance Frequency Analysis in Assessing Implant Stability: A Retrospective Analysis. The International Journal of Prosthodontics 32:317-326

16. Coelho PG, Marin C, Teixeira HS, Campos FE, Gomes JB, Guastaldi F, Anchieta RB, Silveira L, Bonfante EA (2013) Biomechanical evaluation of undersized drilling on implant biomechanical stability at early implantation times. Journal of Oral and Maxillofacial Surgery 71:e69-e75

17. Coyac BR, Leahy B, Salvi G, Hoffmann W, Brunski JB, Helms JA (2019) A preclinical model links osseo-densification due to misfit and osseo-destruction due to stress/strain. Clinical Oral Implants Research 30:1238-1249

18. Dard M, Kuehne S, Obrecht M, Grandin M, Helfenstein J, Pippenger BE (2016) Integrative Performance Analysis of a Novel Bone Level Tapered Implant. Advances in Dental Research 28:28-33

19. Dias DR, Leles CR, Lindh C, Ribeiro-Rotta RF (2016) Marginal bone level changes and implant stability after loading are not influenced by baseline microstructural bone characteristics: 1-year follow-up. Clinical Oral Implants Research 27:1212-1220

20. Donath K, Breuner G (1982) A method for the study of undecalcified bones and teeth with attached soft tissues. The Säge-Schliff (sawing and grinding) technique. Journal of Oral Pathology and Medicine 11:318-326

21. Donati M, La Scala V, Billi M, Di Dino B, Torrisi P, Berglundh T (2008) Immediate functional loading of implants in single tooth replacement: a prospective clinical multicenter study. Clinical Oral Implants Research 19:740-748

22. Donos N, Asche NV, Akbar AN, Francisco H, Gonzales O, Gotfredsen K, Haas R, Happe A, Leow N, Navarro JM, Ornekol T, Payer M, Renouard F, Schliephake H (2021) Impact of timing of dental implant placement and loading: Summary and consensus statements of group 1 – The 6th EAO Consensus Conference 2021. Clinical Oral Implants Research 32:85-92

23. Dorogoy A, Rittel D, Shemtov-Yona K, Korabi R (2017) Modeling dental implant insertion. Journal of the Mechanical Behavior of Biomedical Materials 68:42-50

24. Dos Santos MV, Elias CN, Cavalcanti Lima JH (2011) The effects of superficial roughness and design on the primary stability of dental implants. Clinical Implant Dentistry and Related Research 13:215-223

25. Duyck J, Corpas L, Vermeiren S, Ogawa T, Quirynen M, Vandamme K, Jacobs R, Naert I (2010) Histological, histomorphometrical, and radiological evaluation of an experimental implant design with a high insertion torque. Clinical Oral Implants Research 21:877-884

26. Elias CN, Rocha FA, Nascimento AL, Coelho PG (2012) Influence of implant shape, surface morphology, surgical technique and bone quality on the primary stability of dental implants. Journal of the Mechanical Behavior of Biomedical Materials 16:169-180

27. Eom TG, Kim HW, Jeon GR, Yun MJ, Huh JB, Jeong CM (2016) Effects of different implant osteotomy preparation sizes on implant stability and bone response in the minipig mandible. The International Journal of Oral and Maxillofacial Implants 31:997-1006

28. Fanali S, Tumedei M, Pignatelli P, Inchingolo F, Pennacchietti P, Pace G, Piattelli A (2021) Implant primary stability with an osteocondensation drilling protocol in different density polyurethane blocks. Computer Methods in Biomechanics and Biomedical Engineering 24:14-20

29. Friberg B, Ahmadzai M (2019) A prospective study on single tooth reconstructions using parallel walled implants with internal connection (NobelParallel CC) and abutments with angulated screw channels (ASC). Clinical Implant Dentistry and Related Research 21:226-231

30. Frisardi G, Barone S, Razionale AV, Paoli A, Frisardi F, Tullio A, Lumbau A, Chessa G (2012) Biomechanics of the press-fit phenomenon in dental implantology: an image-based finite element analysis. Head and Face Medicine 8:18

31. Gehrke SA, Pérez-Díaz L, Mazón P, De Aza PN (2019) Biomechanical Effects of a New Macrogeometry Design of Dental Implants: An In Vitro Experimental Analysis. Journal of Functional Biomaterials 10:47

32. Grobecker-Karl T, Orujov K, Klär V, Karl M (2021) Use of a dentin bonding agent for the fixation of strain gauges on bone. Journal of the Mechanical Behavior of Biomedical Materials 119:104545

33. Ikar M, Grobecker-Karl T, Karl M, Steiner C (2020) Mechanical stress during implant surgery and its effects on marginal bone: a literature review. Quintessence International 51:142-150

34. Javed F, Ahmed HB, Crespi R, Romanos GE (2013) Role of primary stability for successful osseointegration of dental implants: Factors of influence and evaluation. Interventional Medicine and Applied Science 5:162-167

35. Karl M, Albrektsson T (2017) Clinical Performance of Dental Implants with a Moderately Rough (TiUnite) Surface: A Meta-Analysis of Prospective Clinical Studies. The International Journal of Oral and Maxillofacial Implants 32:717-734

36. Karl M, Irastorza-Landa A (2017) Does implant design affect primary stability in extraction sites? Quintessence International 48:219-224

37. Karl M, Scherg S, Grobecker-Karl T (2017) Fracture of Reduced-Diameter Zirconia Dental Implants Following Repeated Insertion. The International Journal of Oral and Maxillofacial Implants 32:971-975

38. Karl M, Grobecker-Karl T (2018) Effect of bone quality, implant design, and surgical technique on primary implant stability. Quintessence International 22:189-198

39. Karl M, Palarie V, Nacu V, Chele N, Steiner C, Grobecker-Karl T (2018) Micromotion Phenomena at the Implant Bone Interface: A Biomechanical and Histomorphometric study. Journal of Dental and Maxillofacial Surgery 1:56-63

40. Karl M, Palarie V, Nacu V, Grobecker-Karl T (2020) A Pilot Animal Study Aimed at Assessing the Mechanical Quality of Regenerated Alveolar Bone. The International Journal of Oral and Maxillofacial Implants 35:313-319

41. Klär V, Karl M, Grobecker-Karl T (2022) Bone Damage during Dental Implant Insertion: A Pilot Study Combining Strain Gauge and Histologic Analysis. Applied Sciences 12:291

42. Lages FS, Douglas-de-Oliveira DW, Costa FO (2018) Relationship between implant stability measurements obtained by insertion torque and resonance frequency analysis: A systematic review. Clinical Implant Dentistry and Related Research 20:26-33

43. Lee KJ, Cha JK, Sanz-Martin I, Sanz M, Jung UW (2019) A retrospective case series evaluating the outcome of implants with low primary stability. Clinical Oral Implants Research 30:861-871

44. Lekholm U, Zarb GA (1985) Patient selection and preparation. In Branemark PI, Zarb GA, Albrektsson T (eds) Tissue Integrated Prostheses: Osseointegration in Clinical Dentistry. Quintessence Publishing Co. Inc., Chicago, pp 199-209

45. Lemos CA, Ferro-Alves ML, Okamoto R, Mendonça MR, Pellizzer EP (2016) Short dental implants versus standard dental implants placed in the posterior jaws: A systematic review and meta-analysis. Journal of Dentistry 47:8-17

46. Li Manni L, Lecloux G, Rompen E, Aouini W, Shapira L, Lambert F (2020) Clinical and radiographic assessment of circular versus triangular cross-section neck Implants in the posterior maxilla: A 1-year randomized controlled trial. Clinical Oral Implants Research 31:814-824

47. Menicucci G, Pachie E, Lorenzetti M, Migliaretti G, Carossa S (2012) Comparison of primary stability of straight-walled and tapered implants using an insertion torque device. International Journal of Prosthodontics 25:465-471

48. Misch CE, Perel ML, Wang HL, Sammartino G, Galindo-Moreno P, Trisi P, Steigmann M, Rebaudi A, Palti A, Pikos MA, Schwartz-Arad D, Choukroun J, Gutierrez-Perez JL, Marenzi G, Valavanis DK (2008) Implant success, survival, and failure: the International Congress of Oral Implantologists (ICOI) Pisa Consensus Conference. Implant Dentistry 17:5-15

49. Nicolielo LFP, Van Dessel J, Jacobs R, Quirino Silveira Soares M, Collaert B (2020) Relationship between trabecular bone architecture and early dental implant failure in the posterior region of the mandible. Clinical Oral Implants Research 31:153-161

50. Palombo D, Rahmati M, Vignoletti F, Sanz-Esporrin J, Haugen HJ, Sanz M (2021) Hard and soft tissue healing around implants with a modified implant neck configuration: An experimental in vivo preclinical investigation. Clinical Oral Implants Research 32:1127-1141

51. Trisi P, Berardi D, Paolantonio M, Spoto G, D'Addona A, Perfetti G (2013) Primary stability, insertion torque, and bone density of conical implants with internal hexagon: is there a relationship? The Journal of Craniofacial Surgery 24:841-844

52. Pérez-Pevida E, Cherro R, Camps-Font O, Piqué N (2020) Effects of Drilling Protocol and Bone Density on the Stability of Implants According to Different Macrogeometries of the Implant Used: Results of an In Vitro Study. The International Journal of Oral and Maxillofacial Implants 35:955-964

53. Sotto-Maior BS, Rocha EP, de Almeida EO, Freitas-Júnior AC, Anchieta RB, Del Bel Cury AA (2010) Influence of high insertion torque on implant placement: an anisotropic bone stress analysis. Brazilian Dental Journal 21:508-514

54. Steiner C, Karl M, Grobecker-Karl T (2020) Insertion and Loading Characteristics of Three Different Bone-Level Implants. The International Journal of Oral and Maxillofacial Implants 35:560-565

55. Susarla SM, Chuang SK, Dodson TB (2008) Delayed versus immediate loading of implants: survival analysis and risk factors for dental implant failure. Journal of Oral and Maxillofacial Surgery 66:251-255

56. Swami V, Vijayaraghavan V, Swami V (2016) Current trends to measure implant stability. Journal of Indian Prosthodontic Society 16:124-130

57. Tabassum A, Walboomers XF, Wolke JG, Meijer GJ, Jansen JA (2010) Bone particles and the undersized surgical technique. Journal of Dental Research 89:581-586

58. Tabassum A, Meijer GJ, Walboomers XF, Jansen JA (2011) Biological limits of the undersized surgical technique: a study in goats. Clinical Oral Implants Research 22:129-134

59. Tabassum A, Meijer GJ, Walboomers XF, Jansen JA (2014) Evaluation of primary and secondary stability of titanium implants using different surgical techniques. Clinical Oral Implants Research 25:487-492

60. Taing-Watson E, Katona TR, Stewart KT, Ghoneima A, Chu GT, Kyung HM, Liu SS (2015) Microdamage generation by tapered and cylindrical mini-screw implants after pilot drilling. The Angle Orthodontist 85:859-867

61. Yang B, Irastorza-Landa A, Heuberger P, Ploeg HL (2020) Effect of insertion factors on dental implant insertion torque/energy – experimental results. Journal of the Mechanical Behavior of Biomedical Materials 112:103995

7 Publications

7.1 Original articles

1. Grobecker-Karl T, Orujov K, Klär V, Karl M (2021) Use of a dentin bonding agent for the fixation of strain gauges on bone. J Mech Behav Biomed Mater 119:104545 https://doi.org/10.1016/j.jmbbm.2021.104545

2. Klär V, Karl M, Grobecker-Karl T (2022) Bone Damage during Dental Implant Insertion: A Pilot Study Combining Strain Gauge and Histologic Analysis. Appl Sci 12(1):291 https://doi.org/10.3390/app12010291

(see appendix)

7.2 Poster presentation

Virgilia Klär, Matthias Karl, Tanja Grobecker-Karl. Knochenschädigung im Rahmen der Implantatinsertion - eine biomechanische und histologische Pilotstudie. Posterdemonstration 36. Kongress der Deutschen Gesellschaft für Implantologie DGI (November 2022, Hamburg)

8 Acknowledgement

9 Appendix

<u>Materials used</u>

Implants

Dr. Ihde STO 4.1 × 11 mm	Dr. Ihde Dental GmbH, Eching, Germany
Straumann Bone Level Tapered 4.1 × 12 mm	Institut Straumann AG, Basel, Switzerland
OsseoSpeed TX 4.0 S × 13 mm	Astra Tech Implant System, Dentsply Implants Manufacturing GmbH, Mannheim, Germany

Chemical materials

Ethanol	Ethanol 99% fully denatured; SAV Liquid Production, Flintsbach a. Inn, Germany
Fuchsin	Resolab®, Bad Oeynhausen, Germany
Fluorescent dye	MET-L-CHEK® Penetrant FP 97 A (M); Helling, Heidgraben, Germany
Xylene	Morphisto, Frankfurt am Main, Germany
Cold-curing polymer	ProBase®; Ivoclar Vivadent, Schaan, Liechtenstein
Polymethylmethacrylate	Technovit® 9100; Heraeus Kulzer, Hanau, Germany
Cold-curing polymer (sawing and grinding technique)	Technovit® 4000, Heraeus Kulzer, Hanau, Germany
One component precision adhesive (sawing and grinding technique)	Technovit® 7210 VLC, Heraeus Kulzer, Hanau, Germany
Polyurethane resin	Biresin® G27; Sika Deutschland GmbH, Bad Urach, Germany
Dentin bonding agent	Syntac® Primer, Syntac® Adhesive, Heliobond; Ivoclar Vivadent, Schaan, Liechtenstein

Devices

Diamond band saw	EXAKT 300, EXAKT Advanced Technologies GmbH, Norderstedt, Germany
Precision adhesive press	EXAKT Advanced Technologies GmbH, Norderstedt, Germany
Grinding system	Grinding system TegraPol- 31 (Struers ApS, Ballerup, Denmark
Silicon carbid abrasive paper	WS FLEX 18 C P 320, 800, 1200, 2500 grit sandpaper, Hermes Schleifmittel GmbH, Hamburg, Germany
Surgical motor	iChiropro, BienAir, Biel, Switzerland
Osstell ISQ device	Osstell AB, Gothenburg, Sweden
Vacuum chamber	BACOENG® 1 Gallon Flat Stainless Steel Vacuum and Degassing Chamber, Suzhou Jianli Machinery And Equipment Co., LTD, Suzhou, China
Microscope	LEICA DM4B; LEICA Mikrosysteme Vertrieb GmbH, Wetzlar, Germany
Unidirectional strain gauges	LY11- 0.6/120, 120 Ω reference resistance; Hottinger Baldwin Messtechnik GmbH, Darmstadt, Germany
Solder tags	LS 7; Hottinger Baldwin Messtechnik GmbH, Darmstadt, Germany
Measurement amplifier	Quantum X; Hottinger Baldwin Messtechnik GmbH, Darmstadt, Germany
Analyzing software	jBEAM; AMS GmbH, Chemnitz, Germany
X-ray machine	Faxitron X-ray, Lincolnshire, IL, USA; 14 kV, 0.3 mA, 2.5 min; Insight Dental Film, Carestream Health Inc., Rochester, NY, USA
Color image analyzing system	LEICA Application Suite, LEICA Phase Expert; LEICA Mikrosysteme Vertrieb GmbH, Wetzlar, Germany
R software package	R, The R Foundation for Statistical Computing, Vienna, Austria; www.R-project.org; accessed 18 November 2021

Table 7. *Embedding and staining protocol of the specimens 1-12*

Step	Process	Material	Concentration/ ratio	Specimens	Time
1	Dehydration	Ethanol 99% denatured	70%	All*	1 day
2	Dehydration	Ethanol 99% denatured	70%	All*	1 day
3	Dehydration	Ethanol 99% denatured	80%	7, 8	6 days
	+ Staining	+ fuchsin	1%	(1-6)* and (9-12)*	1 day
4	Dehydration	Ethanol 99% denatured	80%	7, 8	-
	+ Staining	+ fuchsin	1%	(1-6)* and (9-12)*	1 day
5	Dehydration	Ethanol 99% denatured	90%	7, 8	6 days
	+ Staining	+ fuchsin	1%	(1-6)* and (9-12)*	1 day
6	Dehydration	Ethanol 99% denatured	90%	7, 8	-
	+ Staining	+ fuchsin	1%	(1-6)* and (9-12)*	1 day
7	Dehydration	Ethanol 99% denatured	96%	7, 8	-
	+ Staining	+ fuchsin	1%	(1-6)* and (9-12)*	1 day
8	Dehydration	Ethanol 99% denatured	96%	7, 8	-
	+ Staining	+ fuchsin	1%	(1-6)* and (9-12)*	1 day
9	Dehydration	Ethanol 99% denatured	100%	7, 8	6 days
	+ Staining	+ fuchsin	1%	(1-6)* and (9-12)*	1 day
10	Dehydration	Ethanol 99% denatured	100%	7, 8	6 days
	+ Staining	+ fuchsin	1%	(1-6)* and (9-12)*	1 day
11	Rinsing	Ethanol 99% denatured	100%	(1-6)* and (9-12)*	1 hour

12	Intermedium	Xylene	100%	7, 8	3 days
				(1-6)* and (9-12)*	8 hours
13	Embedding	ProBase®		9	7 days
	Preinfiltration I	Technovit® 9100 stabilised	1:1	7, 8	3 days
		Xylene		(1-6)* and (10-12)*	1 day
14	Preinfiltration II	Technovit® 9100 stabilised	200 ml	(1, 4, 10, 11, 12)*	1 day
		Technovit® 9100 hardener 1	1g	2, 5, (7, 8)*	3 days
				3, 6	6 days
15	Preinfiltration III	Technovit® 9100 destabilised	200 ml	(1, 4, 10, 11, 12)*	1 day
		Technovit® 9100 hardener 1	1g	2, 5	3 days
				3, 6	6 days
	+ Staining	MET-L-CHEK®	100 ml	(7, 8)*	3 days
16	Infiltration	Technovit® 9100 destabilised	250 ml	(1, 4, 10, 11, 12)*	1 day
		Technovit® 9100 hardener 1	1g	(2, 5)*	3 days
		Technovit® 9100 PMMA-powder	20 g	(3, 6)*	6 days
				(7, 8)*	3 days
17	Polymerisation	Technovit® 9100 stock solution A	9A:1B	All	7 days
		Technovit® 9100 stock solution B			

* = under vacuum

Article

Bone Damage during Dental Implant Insertion: A Pilot Study Combining Strain Gauge and Histologic Analysis

Virgilia Klär [ORCID], **Matthias Karl** *[ORCID] and **Tanja Grobecker-Karl**

Department of Prosthodontics, Saarland University, 66421 Homburg, Saar, Germany; virgilia.klaer@gmx.de (V.K.); tanja.grobecker-karl@uks.eu (T.G.-K.)

* Correspondence: matthias.karl@uks.eu; Tel.: +49-6841-1624900

Abstract: Besides alveolar bone quality, the drilling protocol applied in conjunction with the design of an implant are the major determinants of primary implant stability. Surgical trauma and bone compression resulting from implant insertion may constitute one cause for marginal bone resorption. Inserting two current bone-level implant designs (Astra; Straumann; $n = 5$) in bovine ribs, primary stability, strain development on the buccal bone plate and histologic signs of bone damage were recorded. Besides comparing the implant designs (Welch t-tests), all measurement parameters were checked for potential correlations (Pearson product moment correlation coefficients) with the level of significance set at $\alpha = 0.05$. Considerable numbers of crack formation and plastic deformation of bone were observed after implant insertion. Straumann implants showed slightly greater values for insertion torque ($p = 0.772$), strain development ($p = 0.893$) and implant stability ($p = 0.642$). Significantly greater bone to implant contact (cortical $p = 0.014$; trabecular $p = 0.016$) was observed in Straumann implants, while Astra implants caused a significantly greater number of microcracks in cortical bone ($p = 0.020$). In Straumann implants, insertion torque correlated with bone to implant contact in the cortical area ($p = 0.029$) and the number of macrocracks in trabecular bone correlated with bone to implant contact ($p = 0.029$). In Astra implants, insertion torque and bone to implant contact in the trabecular area correlated ($p = 0.007$) as well as the number of macrocracks in trabecular bone and implant stability ($p = 0.016$). Additionally, in the area of cortical bone, the number of macrocracks correlated with bone to implant contact ($p = 0.019$). Implant placement results in bone damage of varying magnitude, which is governed by the drill protocol, implant macrodesign and bone quality.

Keywords: implant design; primary implant stability; mechanical trauma; strain development; crack formation

1. Introduction

Alveolar bone consists of cortical and trabecular compartments in varying percent composition resulting in different bone qualities [1,2]. When dental implants are placed, primary stability reducing micromotion at the implant–bone interface in order to ensure osseointegration, has to be achieved. In this context, a clinical study showed that implants with low initial stability bear a higher risk of failure [3].

With shortened treatment protocols, implant manufacturers strive for maximizing primary stability by defining drill protocols depending on the hard to evaluate bone quality, and by designing implants often causing compression especially in the cortical layer of bone [2,4–6]. The exact implications of the factors mentioned are not yet well known with partially contradictive results presented in literature. In an animal study comparing different drill protocols, a correlation between insertion torque and radiographic bone loss after 6 weeks of healing was found with implants achieving greater torque showing more marginal bone loss [7]. On the other hand, a clinical study showed that microstructural bone characteristics had no effect on changes in marginal bone level and implant stability [1]. A

further clinical study found that implant survival was associated with intermediate bone types; the authors concluded that both, very sparse or very dense bone are critical [8].

With marginal bone resorption causing problems with both, esthetics and maintenance, several potential factors, including vertical positioning and implant abutment connection [9,10], governing bone response to dental implant placement have been investigated. Besides establishing biologic width, initial marginal bone loss after implant placement has been described as the result of an adaptive bone response to surgical trauma and implant loading [11]. Based on a recent clinical study including 22 implants, the extent of initial marginal bone loss between implant insertion and prosthetic restoration averages 0.41 mm (SD = 0.45 mm) [12].

As a potential solution to mechanically overloading alveolar bone during implant insertion, implants with a triangular cross-section have been introduced. Following the creation of a round osteotomy, the insertion of a triangular implant with a flat surface oriented buccally would relieve the buccal bone plate. However, two clinical studies did not identify major differences with circular cross-section neck implants [13] apart from somewhat reduced crestal bone loss [14].

It was the goal of this ex vivo experiment to quantify primary implant stability and strain development on the surface of the buccal bone plate during insertion of two current bone-level implant types and to examine potential correlations with histologically assessed bone damage.

2. Materials and Methods

2.1. Biomechanical Measurements

Bovine ribs were freshly obtained from the local slaughterhouse, cut into pieces with a length of 30 mm using a diamond band saw (EXAKT 300, EXAKT Advanced Technologies GmbH, Norderstedt, Germany) and the periosteum was removed completely. The specimens were then embedded in metal holders using polyurethane resin (Biresin G27, Sika Deutschland GmbH, Bad Urach, Germany), which allowed for the stable fixation on a metal plate for handling purposes. All biomechanical study parts were completed in one day in order not to require freezing and thawing.

Following the implant manufacturers' protocols for medium type bone (Table 1), a surgical motor (iChiropro, BienAir, Biel, Switzerland) was used for creating osteotomies with a distance of approximately 2 mm to the cortical plate, simulating the buccal bone surface (Figure 1). In order to ensure perpendicular osteotomies, a metal guide sleeve could be positioned on the top surface of the bone samples. Unidirectional strain gauges (LY11-0.6/120, 120 Ω reference resistance, Hottinger Baldwin Messtechnik GmbH, Darmstadt, Germany) were attached to the bone surface with the sensing element oriented in the mesio-distal direction using a dentin bonding agent [15]. Solder tags (LS 7; Hottinger Baldwin Messtechnik GmbH) were attached to the metal holders using cyanoacrylate followed by usual wiring. A measurement amplifier (Quantum X, Hottinger Baldwin Messtechnik GmbH) and analyzing software (jBEAM, AMS GmbH, Chemnitz, Germany) were used for recording strain development during the insertion of two groups of current bone-level implants (n = 5; Table 1) at a maximum velocity of 25 rpm. Following implant insertion, resonance frequency analysis was performed, both in the mesio-distal and bucco-lingual direction using implant specific smart peg abutments and an Osstell ISQ device (implant stability quotient; Osstell AB, Gothenburg, Sweden).

Table 1. Implant types and drill protocols.

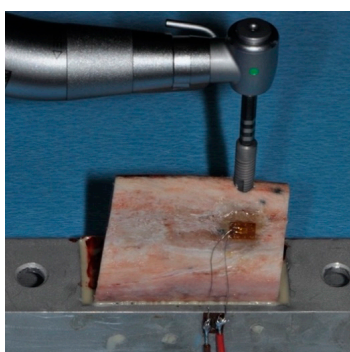| Group Name	Straumann	Astra
Implant	Straumann Bone Level Tapered 4.1 × 12 mm (Institut Straumann AG, Basel, Switzerland)	OsseoSpeed TX 4.0 S × 13 mm (Astra Tech Implant System, Dentsply Implants Manufacturing GmbH, Mannheim, Germany)
Drill sequence	Needle drill 2.2 mm pilot drill 2.8 mm BLT drill 3.5 mm BLT drill	Round bur Twist drill 2.0 Twist drill 3.2 Twist drill 3.7

Figure 1. Insertion of an OsseoSpeed implant in bovine rib bone, which has been positioned in a metal holder and equipped with a strain gauge on the buccal surface. The sensing element of the strain gauge is positioned in the horizontal direction.

2.2. Histologic Analysis

With the implants in place, the specimens were removed from the metal holders by cutting at a distance of 10 mm relative to the surface of the implants using the diamond band saw described above. Subsequently, the specimens were dehydrated in alcohol solutions of increasing concentrations, clarified in xylene and embedded in polymethylmethacrylate (Technovit 9100, Heraeus Kulzer, Hanau, Germany). One sagittal section (Figure 2) parallel to the long axis of the implant and corresponding to the center of the strain gauge was obtained per specimen by a cutting and grinding technique [16]. With the sections reduced to a thickness of 120 μm, microradiographs (Faxitron X-ray, Lincolnshire, IL, USA; 14 kV, 0.3 mA, 2.5 min; Insight Dental Film, Carestream Health Inc., Rochester, NY, USA) were obtained for determining bone mineral density (BMD) in the surrounding of the implants (Figure 3). Following further reduction of the sections to a thickness of 30 μm, bone to implant contact (BIC) and bone damage were quantified histomorphometrically using a microscope (LEICA DM4B, LEICA Mikrosysteme Vertrieb GmbH, Wetzlar, Germany) equipped with a color image analyzing system (LEICA Application Suite, LEICA Phase Expert, LEICA Mikrosysteme Vertrieb GmbH). All measurements were made on images gathered at 20× magnification. Following the outlining of the implant surface (Figure 4a, yellow line) and the internal bony wall of the drill holes (Figure 4a, red line), BIC was defined as bone appearing within a radius of 500 μm surrounding a specific point on the implant surface. The region of interest for evaluating bone damage was defined by circles with a radius of 300 μm surrounding the bony walls at points best representing the outer geometry of the implants (Figure 4b, blue line). Bone damage, as indicated by crack formation or deformation of bone structure, was quantified with cracks exceeding

9 Appendix

100 μm being classified as macrocracks, while cracks with a length shorter than 100 μm were classified as microcracks.

(**a**)   (**b**)
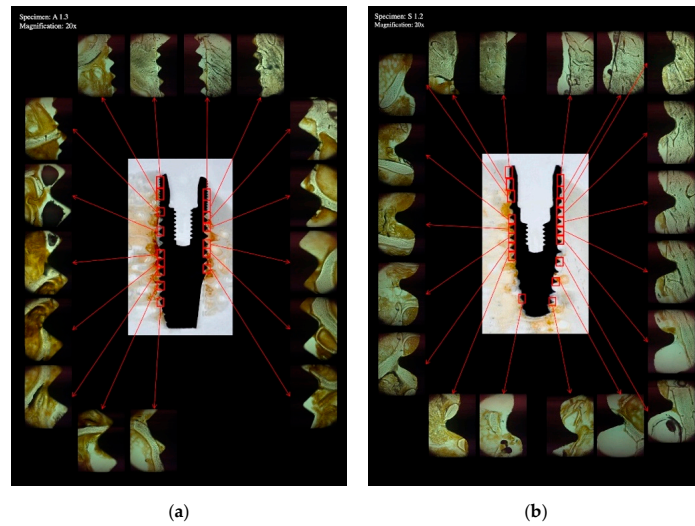
Figure 2. Overview of a histologic section showing an OsseoSpeed (**a**) and a Straumann BLT (**b**) implant placed in bovine rib bone. The implant bone interface was analyzed in varying numbers of images at 20× magnification.
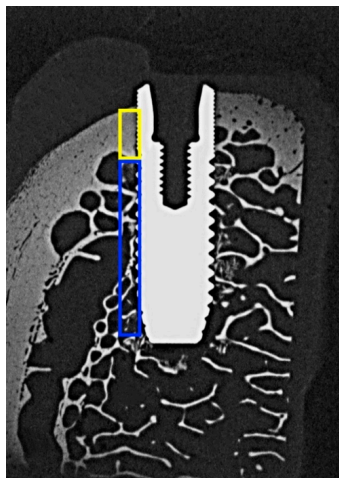
Figure 3. Microradiograph of an OsseoSpeed implant placed in bovine rib bone and sectioned in the bucco-lingual direction. The areas used for determining bone mineral density (BMD) in the cortical and trabecular parts are outlined in yellow and blue color respectively.
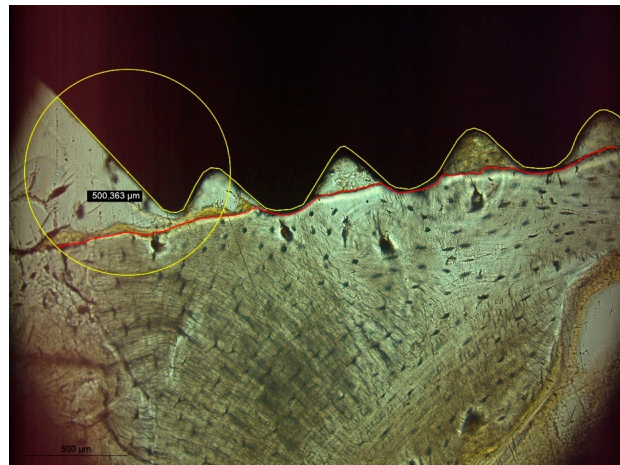
(**a**)

(**b**)

Figure 4. (**a**) BIC was defined as bone being present within a radius of 500 μm surrounding a specific point of the implant surface (yellow line). (**b**) The bony walls of the implant socket were identified (red line) and a radius of 300 μm surrounding a specific point of the bony socket was defined as region of interest for determining bone damage.

2.3. Statistical Analysis

Statistical analysis was based on maximum insertion torque, maximum strain development and mean values of primary implant stability and all histologic parameters, which were separately determined for the cortical and trabecular parts of bone. Following descriptive statistics, Shapiro–Wilk tests on normality of distribution of measurement values were performed, followed by Welch *t*-tests for comparing Astra vs. Straumann implants (n = 5). Pearson product moment correlation coefficients were calculated for evaluating potential correlations among measurement parameters. All calculations were carried out using the R software package (R, The R Foundation for Statistical Computing, Vienna,

3. Results

The mean values and standard deviations for all measurement parameters are given in Table 2. In five instances, the Shapiro–Wilk tests indicated a non-normal distribution of measurement values (Table 2). Only in three comparisons between implant types, a significant difference could be observed (Table 2).

Table 2. Descriptive statistics and pairwise comparisons of the two implant types investigated. Significant differences between groups ($p < 0.05$) are written in bold.

	ASTRA		Straumann		Welch *t*-Tests (*p*-Value)
	Mean	**SD**	**Mean**	**SD**	
Torque	29.76	26.893	34.08	17.428	0.772
Strain	383.38	299.860	410.84	284.754	0.893
ISQ	* 79.20	11.339	81.80	2.842	0.642
BMDc	0.894	0.025	0.872	0.058	0.466
BMDt	0.486	0.099	0.434	0.065	0.360
BICc	0.756	0.059	0.868	0.054	**0.014**
BICt	0.428	0.064	0.600	0.101	**0.016**
microC	** 92.204	26.241	49.732	7.318	**0.020**
microT	*** 44.484	18.810	**** 45.034	23.733	0.969
macroC	10.862	1.443	11.020	2.073	0.893
macroT	5.494	0.976	6.286	3.045	0.600
defC	0.592	0.504	0.326	0.195	0.320
defT	0.368	0.161	***** 0.418	0.226	0.699

p-values of Shapiro–Wilk tests indicating a non-normal distribution of measurement values: * 0.014; ** 0.019; *** 0.050; **** 0.028; ***** 0.004. Abbreviations and units: Torque [Ncm]: implant insertion torque; Strain [μm/m]: strain development on buccal bone; ISQ [no physical unit]: implant stability quotient; BMDc [%]: bone mineral density in the cortical area; BMDt [%]: bone mineral density in the trabecular area; BICc [%]: bone to implant contact in the cortical area; BICt [%]: bone to implant contact in the trabecular area; microC [quantity]: total number of microcracks detected in cortical bone; microT [quantity]: total number of microcracks detected in trabecular bone; macroC [quantity]: number of macrocracks detected in cortical bone; macroT [quantity]: number of macrocracks detected in trabecular bone; defC [quantity]: total number of deformed bone areas detected in cortical bone; defT [quantity]: total number of deformed bone areas in trabecular bone.

Slightly higher insertion torque ($p = 0.772$), strain development ($p = 0.893$) and implant stability ($p = 0.642$) were seen in Straumann implants but did not significantly differ from Astra implants. As expected, bone mineral density in the cortical ($p = 0.466$) and trabecular ($p = 0.360$) area did not differ between groups.

Significantly greater bone to implant contact was observed in Straumann implants, both in cortical ($p = 0.014$) and trabecular ($p = 0.016$) areas. However, Astra implants caused a significantly greater number of microcracks in cortical bone ($p = 0.020$). No further significant differences with respect to bone damage were observed between the groups.

In general, only a few and weak correlations were seen between the different parameters recorded (Table 3). In Straumann implants, insertion torque correlated with bone to implant contact in the cortical area ($p = 0.029$), while in trabecular bone, the number of macrocracks correlated with bone to implant contact ($p = 0.029$). In Astra implants, a correlation between insertion torque and bone to implant contact in the trabecular area was found ($p = 0.007$) as well as a correlation between the number of macrocracks in trabecular

bone and implant stability (p = 0.016). Additionally, in the area of cortical bone, the number of macrocracks correlated with bone to implant contact (p = 0.019).

Table 3. (**a**) Pearson product moment correlation coefficients for measurement parameters recorded in ASTRA implants. (**b**) Pearson product moment correlation coefficients for measurement parameters recorded in Straumann implants.

(a)												
										Correlation Coefficients		
	Torque	**Strain**	**ISQ**	**BMDc**	**BMDt**	**BICc**	**BICt**	**microC**	**microT**	**macroC**	**macroT**	**defC**	**defT**
Torque		−0.239	0.665	0.635	0.867	−0.431	0.969	−0.259	−0.212	−0.502	0.726	0.179	0.549
Strain	0.761		0.511	0.443	0.300	0.859	0.013	0.861	0.745	0.870	−0.700	−0.566	−0.902
ISQ	0.221	0.490		0.664	0.762	0.003	0.665	0.093	0.393	0.107	0.943	0.313	0.006
BMDc	0.250	0.557	0.222		0.652	0.385	0.782	−0.007	0.003	0.220	0.503	0.339	−0.115
BMDt	0.057	0.700	0.134	0.233		−0.128	0.896	0.251	0.270	−0.105	0.685	−0.173	0.119
BICc	0.469	0.141	0.996	0.522	0.838		−0.207	0.559	0.459	0.937	−0.305	−0.095	−0.911
BICt	0.007	0.987	0.220	0.118	0.039	0.738		−0.140	−0.152	−0.320	0.650	0.135	0.369
microC	0.674	0.140	0.882	0.992	0.684	0.327	0.823		0.885	0.721	−0.171	−0.773	−0.809
microT	0.732	0.255	0.513	0.997	0.660	0.437	0.807	0.046		0.718	0.180	−0.485	−0.743
macroC	0.329	0.130	0.864	0.722	0.867	0.019	0.599	0.169	0.172		−0.194	−0.200	−0.983
macroT	0.165	0.230	0.016	0.388	0.202	0.618	0.236	0.783	0.772	0.755		0.439	0.310
defC	0.774	0.434	0.609	0.577	0.780	0.879	0.828	0.125	0.408	0.746	0.460		0.370
defT	0.338	0.098	0.993	0.854	0.849	0.032	0.541	0.098	0.150	0.003	0.612	0.540	
	p-values												

(b)												
										Correlation Coefficients		
	Torque	**Strain**	**ISQ**	**BMDc**	**BMDt**	**BICc**	**BICt**	**microC**	**microT**	**macroC**	**macroT**	**defC**	**defT**
Torque		−0.138	0.040	0.120	0.237	−0.916	0.458	−0.308	0.483	0.498	0.681	−0.036	−0.764
Strain	0.825		0.023	0.624	0.578	0.351	−0.560	−0.235	−0.164	−0.048	−0.252	0.673	−0.480
ISQ	0.949	0.970		0.362	0.335	0.301	−0.600	0.618	−0.819	0.608	−0.597	0.699	−0.115
BMDc	0.848	0.261	0.550		0.992	0.156	−0.754	0.434	−0.127	0.701	−0.472	0.852	−0.327
BMDt	0.701	0.307	0.582	0.001		0.031	−0.672	0.394	−0.039	0.748	−0.372	0.810	−0.394
BICc	0.029	0.562	0.623	0.803	0.960		−0.737	0.435	−0.739	−0.251	−0.868	0.415	0.545
BICt	0.438	0.326	0.285	0.141	0.214	0.155		−0.656	0.676	−0.403	0.915	−0.884	−0.118
microC	0.615	0.703	0.266	0.466	0.512	0.464	0.230		−0.499	0.629	−0.791	0.440	0.520
microT	0.410	0.792	0.090	0.839	0.950	0.154	0.211	0.392		−0.100	0.777	−0.586	−0.139
macroC	0.394	0.939	0.277	0.187	0.146	0.684	0.502	0.255	0.873		−0.256	0.576	−0.272
macroT	0.206	0.682	0.288	0.423	0.537	0.056	0.029	0.111	0.122	0.677		−0.655	−0.473
defC	0.954	0.213	0.189	0.067	0.097	0.487	0.047	0.459	0.299	0.310	0.230		−0.346
defT	0.133	0.414	0.854	0.591	0.512	0.342	0.851	0.370	0.756	0.658	0.421	0.569	
	p-values												

4. Discussion

Considerable numbers of crack formation and plastic deformation of bone have been shown as a consequence of implant site preparation and implant insertion. While exact thresholds for bone damage are unknown, bone resorption as a consequence of mechanical trauma may originate from such regions. Consequently, marginal bone loss of up to 1 mm in the first year after implant placement is still widely accepted as success criterion [11,12].

Based on biomechanical parameters, Straumann implants showed a trend towards greater primary stability as compared to Astra implants. In agreement with this finding,

greater values of bone to implant contact, both in cortical and trabecular areas of bone, were seen in Straumann implants. While the insertion torque of Straumann implants correlated with bone to implant contact in the cortical area, for Astra implants, a correlation for insertion torque with bone to implant contact in trabecular bone was observed. Macrocracks in trabecular bone correlated with bone to implant contact in Straumann implants but with implant stability in Astra implants. Furthermore, Straumann implants caused less microcracks in cortical bone as compared to Astra implants, for which bone to implant contact in cortical bone correlated with the number of macrocracks detected. Given that bone mineral density did not significantly differ between Straumann and Astra specimens, it appears that the implants tested here derive primary stability by engaging different areas of bone [2,5]. Differences in thread design in the cervical area in combination with the drill protocols used here obviously result in less cortical bone damage in Straumann implants as compared to Astra implants.

Only a few and weak correlations among measurement parameters were observed in this study, which has previously also been experienced by other authors [5]. This may be due to the fact that clinical measurements, such as insertion torque and implant stability are rather global in nature, while histologic analysis focusses on very specific parts of the implant bone interface.

The study at hand used two dental implant systems differing in length, diameter, thread pitch and drill protocol. Instead of standardizing, e.g., implant site preparation with respect to undersizing the osteotomy [6,7], the manufacturers' guidelines were applied in order to best reflect clinical practice. While not reported here, this also resulted in different vertical start positions for implant insertion and varying amounts of time required for the insertion process despite a standardized insertion velocity.

As with every in vitro investigation, several limiting factors have to be considered when interpreting the results. For analyzing bone damage, no staining was carried out here based on preliminary tests with toluidine blue staining [17] and fluorescent dye [18], as native bone resulted in the best visual appearance of cracks and deformed bone areas. However, originally basic fuchsin staining has been described as being necessary for analyzing bone damage [19]. Bone to implant contact is normally defined as intimate contact between dental implant and bone during or after healing. In this study, BIC was defined as an area in which surgical trauma caused by implant site preparation or implant insertion may have caused bone damage. Based on an initial screening of the specimens, a radius of 500 μm surrounding a specific point of an implant was chosen while a radius of 300 μm centered at the bony wall of an implant socket was chosen as area of interest for determining bone damage. Wide variation was seen in the measurements performed, which at least partially has to be attributed to the bone material used being characterized by varying thickness of cortical bone. With the insertion characteristics of dental implants also depending on surface characteristics, each implant was used only once. Reducing the effect of varying bone morphology would have required a much greater sample size, which seemed not to be feasible for a pilot study. For comparative biomechanical studies employing different implant systems, a greater level of standardization should be implemented, e.g., by using foam materials as bone surrogate material [4].

Due to the limited sample size chosen in this pilot investigation, normal distribution of measurement values may not be guaranteed even if the Shapiro–Wilk test indicated $p > 0.05$. Both Welch t-tests for pairwise comparisons and Pearson product moment correlation coefficients are not very sensitive with respect to a violation of normal distribution of measurement values. Under this assumption, non-parametric tests seemed not to be required for statistical analysis. Furthermore, the statistical power achieved with the given sample size was low (<0.8), with the exception of the parameters BICt and microC. This does not affect differences which were found to be significant but may obscure non-significant differences as errors of second order.

5. Conclusions

Implant placement employing currently available systems and drill protocols inevitably results in bone damage of varying magnitude. The amount of undersizing an osteotomy relative to the implant diameter seems to be critical and greater primary stability can be associated to greater levels of damage. The macrodesign of an implant determines which areas of bone are being engaged and consequently, novel implant designs should preferably derive stability from trabecular bone while avoiding bone damage in cortical areas. Further benefit could be derived from drill protocols requiring less removal of alveolar bone.

Author Contributions: Conceptualization: T.G.-K.; Methodology: T.G.-K. and V.K.; Formal analysis: M.K.; Data curation: T.G.-K. and V.K.; Writing—original draft preparation: V.K. and M.K.; Writing—review and editing: T.G.-K. and V.K. All authors have read and agreed to the published version of the manuscript.

Institutional Review Board Statement: Not applicable.

Informed Consent Statement: Not applicable.

Conflicts of Interest: The authors declare no conflict of interest.

References

1. Dias, D.R.; Leles, C.R.; Lindh, C.; Ribeiro-Rotta, R.F. Marginal bone level changes and implant stability after loading are not influenced by baseline microstructural bone characteristics: 1-year follow-up. *Clin. Oral Implant. Res.* **2016**, *27*, 1212–1220. [CrossRef] [PubMed]
2. Gehrke, S.A.; Pérez-Díaz, L.; Mazón, P.; De Aza, P.N. Biomechanical Effects of a New Macrogeometry Design of Dental Implants: An In Vitro Experimental Analysis. *J. Funct. Biomater.* **2019**, *10*, 47. [CrossRef] [PubMed]
3. Chen, M.H.; Lyons, K.; Tawse-Smith, A.; Ma, S. Resonance Frequency Analysis in Assessing Implant Stability: A Retrospective Analysis. *Int. J. Prosthodont.* **2019**, *32*, 317–326. [CrossRef] [PubMed]
4. Pérez-Pevida, E.; Cherro, R.; Camps-Font, O.; Piqué, N. Effects of Drilling Protocol and Bone Density on the Stability of Implants According to Different Macrogeometries of the Implant Used: Results of an In Vitro Study. *Int. J. Oral Maxillofac. Implant.* **2020**, *35*, 955–964. [CrossRef] [PubMed]
5. Dard, M.; Kuehne, S.; Obrecht, M.; Grandin, M.; Helfenstein, J.; Pippenger, B.E. Integrative Performance Analysis of a Novel Bone Level Tapered Implant. *Adv. Dent. Res.* **2016**, *28*, 28–33. [CrossRef] [PubMed]
6. Gazelakis, E.; Judge, R.B.; Palamara, J.E.A. The biomechanical profile of an osseo-integrated rectangular block implant: A pilot in vivo experimental study. *Clin. Oral Implant. Res.* **2021**, *32*, 1274–1287. [CrossRef] [PubMed]
7. Abrahamsson, I.; Carcuac, O.; Berglundh, T. Influence of implant geometry and osteotomy design on early bone healing: A pre-clinical in vivo study. *Clin. Oral Implant. Res.* **2021**, *32*, 1190–1199. [CrossRef] [PubMed]
8. Nicolielo, L.F.P.; Van Dessel, J.; Jacobs, R.; Quirino Silveira Soares, M.; Collaert, B. Relationship between trabecular bone architecture and early dental implant failure in the posterior region of the mandible. *Clin. Oral Implant. Res.* **2020**, *31*, 153–161. [CrossRef] [PubMed]
9. Agustín-Panadero, R.; Martínez-Martínez, N.; Fernandez-Estevan, L.; Faus-López, J.; Solá-Ruíz, M.F. Influence of Transmucosal Area Morphology on Peri-Implant Bone Loss in Tissue-Level Implants. *Int. J. Oral Maxillofac. Implant.* **2019**, *34*, 947–952. [CrossRef] [PubMed]
10. Palombo, D.; Rahmati, M.; Vignoletti, F.; Sanz-Esporrin, J.; Haugen, H.J.; Sanz, M. Hard and soft tissue healing around implants with a modified implant neck configuration: An experimental in vivo preclinical investigation. *Clin. Oral Implant. Res.* **2021**, *32*, 1127–1141. [CrossRef] [PubMed]
11. Albrektsson, T.; Chrcanovic, B.; Östman, P.O.; Sennerby, L. Initial and long-term crestal bone responses to modern dental implants. *Periodontol. 2000* **2017**, *73*, 41–50. [CrossRef] [PubMed]
12. Friberg, B.; Ahmadzai, M. A prospective study on single tooth reconstructions using parallel walled implants with internal connection (NobelParallel CC) and abutments with angulated screw channels (ASC). *Clin. Implant. Dent. Relat. Res.* **2019**, *21*, 226–231. [CrossRef] [PubMed]

9 Appendix

13. Li Manni, L.; Lecloux, G.; Rompen, E.; Aouini, W.; Shapira, L.; Lambert, F. Clinical and radiographic assessment of circular versus triangular cross-section neck Implants in the posterior maxilla: A 1-year randomized controlled trial. *Clin. Oral Implant. Res.* **2020**, *31*, 814–824. [CrossRef] [PubMed]
14. Tokuc, B.; Kan, B. The effect of triangular cross-section neck design on crestal bone stability in the anterior mandible: A randomized, controlled, split-mouth clinical trial. *Clin. Oral Implant. Res.* **2021**, *32*, 1241–1250. [CrossRef] [PubMed]
15. Grobecker-Karl, T.; Orujov, K.; Klär, V.; Karl, M. Use of a dentin bonding agent for the fixation of strain gauges on bone. *J. Mech. Behav. Biomed. Mater.* **2021**, *119*, 104545. [CrossRef] [PubMed]
16. Donath, K.; Breuner, G. A method for the study of undecalcified bones and teeth with attached soft tissues. The Säge-Schliff (sawing and grinding) technique. *J. Oral Pathol.* **1982**, *11*, 318–326. [CrossRef] [PubMed]
17. Karl, M.; Palarie, V.; Nacu, V.; Grobecker-Karl, T. A Pilot Animal Study Aimed at Assessing the Mechanical Quality of Regenerated Alveolar Bone. *Int. J. Oral Maxillofac. Implant.* **2020**, *35*, 313–319. [CrossRef] [PubMed]
18. Grobecker-Karl, T.; Christian, M.; Karl, M. Effect of endodontic access cavity preparation on monolithic and ceramic veneered zirconia restorations. *Quintessence Int.* **2016**, *47*, 725–729. [PubMed]
19. Burr, D.B.; Hooser, M. Alterations to the en bloc basic fuchsin staining protocol for the demonstration of microdamage produced in vivo. *Bone* **1995**, *17*, 431–433. [CrossRef]

10 Curriculum vitae

Aus datenschutzrechtlichen Gründen wird der Lebenslauf in der elektronischen Fassung der Dissertation nicht veröffentlicht.